Journal of Molecular Liquids xxx (xxxx) 118850

Contents lists available at ScienceDirect

Journal of Molecular Liquids

journal homepage: www.elsevier.com/locate/molliq

Influence of the cation partner on levulinate ionic liquids properties

Angelica Mero [a], Luca Guglielmero [a, c], Felicia D'Andrea [a], Christian S. Pomelli [a], Lorenzo Guazzelli [a], Spyridon Koutsoumpos [b], George Tsonos [b], Ilias Stavrakas [b], Konstantinos Moutzouris [b], Andrea Mezzetta [a, *]

[a] Università di Pisa, Dipartimento di Farmacia, via Bonanno 6, 56126 Pisa, Italy
[b] Laboratory of Electronic Devices and Materials, Department of Electrical and Electronic Engineering, University of West Attica, Egaleo 12244, Greece
[c] University of Pisa, DESTEC, Largo Lucio Lazzarino, 56122 Pisa, Italy

ARTICLE INFO

Article history:
Received 28 September 2021
Received in revised form 2 January 2022
Accepted 28 February 2022

Keywords:
Levulinate ionic liquids
Bio-based ionic liquids
Thermal behaviour
Viscosity
Density
Refractive index
Fragility index

ABSTRACT

In the context of bio-based ionic liquids (ILs), in recent years levulinate ILs have been explored in various applications with appreciable performances. To expand their scope of use, seven selected levulinate ILs featuring different cationic moieties have been prepared and their physico-chemical properties compared. While all the ILs generated displayed only glass transitions at low temperature (< −60 °C), $[C_4C_1Pyr]$Lev presented melting and crystallization events. The thermal stability determined by TGA decreased in the order $[P_{8881}]$Lev > $[C_2C_1Im]$Lev ≈ $[C_4C_1Im]$Lev > $[C_2C_1Pip]$Lev > $[C_2C_1Pyr]$Lev ≈ $[C_4C_1Pyr]$Lev > $[N_{8881}]$Lev, and is in good agreement with the general trend observed for carboxylate ILs. In terms of viscosity, the LevILs showed a Newtonian behaviour when considering the shearing rates range, with a marked reduction of the viscosity at increasing temperatures. The glassy behaviour of LevILs was further ascertained applying the MYEGA viscosity-based model for the determination of the fragility index.

The density of the LevILs was found to vary in the vicinity of $1 g/cm^3$, and the systematic refractive index increase with increasing density was identified as a general trend. The refractive index was experimentally determined at five different wavelengths and several temperatures between 80 °C and 130 °C and followed the order $[C_2C_1Im]$Lev > $[C_2C_1Pip]$Lev > $[C_4C_1Im]$Lev > $[C_2C_1Pyr]$Lev > $[C_4C_1Pyr]$Lev > $[P_{8881}]$Lev > $[N_{8881}]$Lev. Overall, the possibility to tune the physico-chemical properties of ILs through structural variations of the cationic part has been proven valid for the LevIL family. When compared with the carboxylate ILs described in the literature, LevILs show great potential for further applicative studies.

1. Introduction

Ionic liquids (ILs) are often referred to as designer media due to the possibility of customising their physico-chemical properties for an application of interest through judicious structural modifications. An IL is an organic salt characterized by a melting point below 100 °C.[1] A great variety of cations and anions may be paired to give rise to structures which respond to these requirements but, interestingly, these can be characterized by different and even opposite nature, i.e. hydrophobic ILs versus hydrophilic ILs.[2-4] This tuneable feature, in conjunction with peculiar properties such as the null vapour pressure,[5] the wide electrochemical window,[6] the high thermal and chemical stability,[7, 8] has made of the ILs a subject of intense research in the last twenty years. For instance, ILs have been investigated as solvents and catalysts for organic transformations,[9,10] in analytical applications,[11,12] for the production of chemicals and materials from biomasses,[13-15] and in pharmaceutical applications.[16-18] It is also worth noting that beyond the academic interest, ILs have reached the industrial level and are nowadays key ingredients in a variety of bulk processes. [19].

However, investigations aimed at evaluating the (eco)toxicity and biodegradability of ILs highlighted the environmental impact and the safety issues associated with their use and concluded that caution should be used when claiming ILs as green materials.[20-22] Furthermore, the vast majority of components which constitute ILs are of petrochemical origin, thus raising the additional concern of their non-renewable character.[23].

In view of facilitating the transition towards sustainable chemistry and as a way to ameliorate the safety and green profile of ILs, a great deal of attention has been devoted recently to the development of bio-based ILs.[24] Indeed, several natural and natural-derived compounds, such as amino acids,[25] fatty acids[25] and lignin,[26] have been ex-

* Corresponding author.
E-mail address: andrea.mezzetta@unipi.it (A. Mezzetta).

https://doi.org/10.1016/j.molliq.2022.118850
0167-7322/© 20XX

ploited for the preparation of this subset of ILs. In this context, sugars arguably represent the most promising pool of natural compounds in terms of availability, structural diversity and potential for modification. [27] Several literature reports describe the direct transformation of monosaccharides in suitable cations and anions,[28] which sometimes require unappealingly long synthetic strategies.[29] On the contrary, the neutralization reaction involving uronic acids[30] or glucosamine [31] represents the most straightforward strategy for the preparation of sugar-derived ILs to date. Interestingly, it has been recently showed that the toxicity towards Zebrafish embryos of a traditional imidazolium IL was reduced when the cation was linked to a sugar pendant. [32] Polysaccharides, i.e. cellulose and hemicellulose, are also valuable sources of compounds for the development of bio-based ILs when converted into smaller molecules such as formic acid, acetic acid, levulinic acid, furfural and hydroxymethyl furfural.[33-36] While formate and acetate ILs have been known for more than twenty years, the utilization of the other mentioned platform chemicals for ILs preparation is far more recent. In particular, for furfural and hydroxymethyl furfural a very limited number of studies have been reported.[37,38].

Conversely, Levulinate ILs have been studied in different applications such as for the extraction of pharmaceuticals via aqueous biphasic systems (ABS),[39] as potential media for CO_2 absorption,[40-42] in asymmetric hydrogenation catalysis,[43] and for cellulose dissolution and modification.[44-46] Moreover, a series of levulinate ILs have been proven non-toxic toward several aquatic species.[46] An increment in toxicity was registered when cations with pronounced hydrophobic nature were tested. It is also worth mentioning that the levulinate moiety represents one of the few carboxylate anions featuring an additional functional group (the carbonyl group), which can participate in further reactions and turn this anion into a task-specific one. Despite this, the properties of levulinate ILs have not yet been thoroughly and comparatively assessed. For a full exploitation of new bio-based media, it is of primary importance to ascertain the thermophysical properties of these promising materials. In order to develop efficient ILs-based processes, it is critical to establish the liquid range of a medium, the maximum allowed temperature that avoids degradation, and the transport properties such as dynamic viscosity and density. Furthermore, the study of the optical features such as the refractive index is critical for the characterisation of the materials and their purity, providing information on the intermolecular forces within a liquid as well as its microwave absorption potential.

In this work, the preparation and study of a series of levulinate-based ILs characterised by various cationic moieties are reported. This set of compounds was designed with the intention of investigating the effect of the nature and structure of their cationic part on the ILs' physicochemical properties. As a result, the thermal stability, thermal behaviour, viscosity, density and refractive index have been assessed and analysed.

2. Material and methods

Materials

If not noted otherwise, reactants and reagents were commercially available and used as received. 1-bromoethane (99%), *N*-methylpyrrolidine (98%), and *N*-methylpiperidine (98%) were purchased from Acros Organics Thermo Fisher (Germany), 1-bromobutane (99 + %) from Alfa Aesar, Thermo Fisher (Germany) and all the solvents from Sigma Aldrich (Merck Life Science). 1-Ethyl-3-methylimidazolium [C_2C_1Im] (98%), 1-butyl-3-methylimidazolium [C_4C_1Im] (98%), trioctylmethylammonium [N_{8881}] (98%) and trioctylmethylphosphonium [P_{8881}] (98%) methylcarbonate methanol solutions were purchased from Proionic GmbH (Austria).

General methods

2.1. Synthesis of Lev ILs from methylcarbonate ILs (1, 2, 6, 7)

1-Ethyl-3-methylimidazolium levulinate [C_2C_1Im]Lev (1) 1-butyl-3-methylimidazolium levulinate [C_4C_1Im]Lev (2), trioctylmethylammonium levulinate [N_{8881}]Lev (6) and trioctylmethylphosphonium levulinate [P_{8881}]Lev (7) were synthetized form methylcarbonate precursors following our previously reported procedure.[46] To a commercial methanolic solution of a proper methylcarbonate IL, levulinic acid (1 equiv) was added. The concentrations of methylcarbonate ILs in methanol solutions were previously determined by volumetric titration using a standard 0,1 M HCl solution (Eutech pH meter, pH 700, calibrated with three standard buffer solutions at pH 4.01, 7.00, and 10.00). The resulting mixture was stirred at room temperature for 2 h and the solvent was evaporated at 60 °C for 12 h under reduced pressure to afford a light-yellow liquid in quantitative yield. ^{1}H and ^{13}C NMR, and FTIR spectra were in agreement with those reported.

2.2. Synthesis of Lev ILs using an ion exchange resin (3–5)

1-Ethyl-1-methylpyrrolidinium levulinate [C_2C_1Pyr]Lev (3), 1-butyl-1-methylipyrrolidinium levulinate [C_4C_1Pyr]Lev (4), and 1-ethyl-1-methylpiperidinium levulinate [C_2C_1Pip]Lev (5) were synthetized from bromide precursors by metathesis reaction with ion exchange resin following the procedure reported in our previous work.[47] The Amberlite IRA400 ion exchange resin (100 g) was activated by suspending it in an aqueous NaOH solution (4% w/w, 500 mL) for 24 h at room temperature. The pretreated resin was packed into a 3.5 cm diameter column and conditioned with 300 mL of NaOH solution (4% w/w). The column was then washed with water until neutrality.

The selected bromide IL (18.6 mmol) was dissolved in 7:3 (v/v) CH_3OH-water (100 mL) and the solution was passed through the column three times. The hydroxyl-bromide substitution was followed by checking the presence of bromide in the eluted solution using silver nitrate solution ($AgNO_3$ test). The test entails acidifying the sample with dilute nitric acid (0.1 N) and then treating it with $AgNO_3$ in order to exclude the presence of Br anions above a concentration of about 10^{-7} mol/L. The column was then washed with 200 mL of CH_3OH/water solution. A solution of levulinic acid (18.6 mmol) in 7:3 (v/v) CH_3OH-water (50 mL) was added under stirring to the prepared hydroxide IL solution. After 1 h at room temperature, the solvent was evaporated at 60 °C for 12 h under reduced pressure affording, after drying in vacuo, the yellowish liquids. All synthetized compounds have been characterized by ^{1}H and ^{13}C NMR and FTIR analyses and all the spectra are provided in the Supporting Information (Figs. S1–S3 for ^{1}H and ^{13}C NMR and Figs. S4–S6 for FTIR).

*2.2.1. 1-Ethyl-1-methylpyrrolidinium levulinate [C_2C_1Pyr]Lev **(3)***

The preparation of **3** (96% yield, yellowish liquid) was performed according to the general procedure. ^{1}H NMR (D_2O) δ 3.48–3.43 (m, 4H, 2 × CH_2CH_2N), 3.38 (q, 2H, J = 7.3 Hz, CH_3CH_2N), 2.99 (s, 3H, CH_3N), 2.76 (t, 2H, J = 6.8 Hz CH_2COCH_3), 2.40 (t, 2H, J = 6.8 Hz, CH_2COO^-), 2.19 (s, 3H, CH_3CO), 2.18–2.16 (m, 4H, 2 × CH_2CH_2N), 1.35 (tt, 3H, J = 7.3 Hz, $J_{H,N}$ = 2 Hz, NCH_2CH_3); ^{13}C NMR (D_2O) δ 214.6 (CO), 180.3 (COO^-), 60.6 (2 × CH_2CH_2N), 58.9 (CH_3CH_2N), 47.0 (CH_3N), 39.1 (CH_2COCH_3), 30.5 (CH_3CO), 29.3 (CH_2COO^-), 20.7 (CH_2CH_2N), 19.6 (CH_2CH_2N), 6.8 (NCH_2CH_3).

2.2.2. 1-Butyl-1-methylpyrrolidinium levulinate [C_4C_1Pyr]Lev (4)

The preparation of **4** (97% yield, yellowish liquid) was performed according to the general procedure. ^{1}H NMR (D_2O) δ 3.51–3.46 (m, 4H, 2 × CH_2CH_2N), 3.33–3.29 (m, 2H, CH_3CH_2N), 3.02 (s, 3H, CH_3N), 2.77 (t, 2H, J = 6.8 Hz CH_2COCH_3), 2.41 (t, 2H, J = 6.8 Hz, CH_2COO^-), 2.21 (s, 3H, CH_3CO), 2.20–2.18 (m, 4H, 2 × CH_2CH_2N), 1.81–1.73 (m, 2H, $CH_3CH_2CH_2$) 1.42–1.33 (m, 2H, $CH_3CH_2CH_2$), 0.96–0.92 (3H, J = 7.4 Hz, $CH_3CH_2CH_2$); ^{13}C NMR (D_2O) δ 214.9 (CO), 180.8 (COO^-),

64.3 (2 × CH_2CH_2N), 64.2 (CH_3CH_2N), 48.1 (CH_3N), 39.4 (CH_2COCH_3), 30.9 (CH_3CO), 29.3 (CH_2COO^-), 25.2 ($CH_3CH_2CH_2$), 21.4 (2 × CH_2CH_2N), 19.3 ($CH_3CH_2CH_2$), 12.9 (NCH_2CH_3).

2.2.3. 1-Ethyl-1-methylpiperidinium levulinate [C_2C_1Pip]Lev (5)

The preparation of **5** (94% yield, yellowish liquid) was performed according to the general procedure. ^{1}H NMR (D_2O) δ 3.36 (q, 2H, J = 7.3 Hz, CH_3CH_2N), 3.27 (t, 4H, J = 5.8 Hz, 2 × CH_2CH_2N), 2.95 (s, 3H, CH_3N), 2.74 (t, 2H, J = 6.8 Hz CH_2COCH_3), 2.38 (t, 2H, J = 6.8 Hz, CH_2COO^-), 2.17 (s, 3H, CH_3CO), 1.85–1.79 (m, 4H, 2 × CH_2CH_2N), 1.69–1.53 (m, 2H, $CH_3CH_2CH_2$) 1.28 (tt, 3H, J = 7.3 Hz, $J_{H,N}$ = 2.0 Hz, CH_3CH_2N); ^{13}C NMR (D_2O) δ 214.6 (CO), 180.3 (COO^-), 60.6 (2 × CH_2CH_2N), 58.9 (CH_3CH_2N), 47.0 (CH_3N), 39.2 (CH_2COCH_3), 30.7 (CH_3CO), 29.3 (CH_2COO^-), 20.7 ($CH_2CH_2CH_2N$), 19.6 (2 × $CH_2CH_2CH_2N$), 6.8 (NCH_2CH_3).

2.3. NMR spectroscopy

^{1}H NMR spectra were recorded in D_2O with a Bruker AVANCE II operating at 400 MHz.. ^{13}C NMR spectra were recorded at 100 MHz. The experiments were performed at 25 °C using 50 mg/mL as sample concentration. The following abbreviations are used: s = singlet, d = doublet, t = triplet, q = quartet, m = multiplet, tt = tripletriplet. The chemical shift (δ) was referenced to the chemical shift of D_2O (δ_H 4.79) and J-values are given in Hz.

2.4. Fourier transform infrared spectroscopy (FTIR)

The ATR-FTIR spectra were recorded with an Agilent Technologies IR Cary 660 FTIR spectrophotometer using macro-ATR accessory a Diamond crystal. The spectra were measured in a range from 4000 to 500 cm^{-1} with 32 scans. The moisture and CO_2 were eliminated from the samples by measuring first the background spectra before each sample.

2.5. Water content determination

The water content of LevILs was estimated by Karl Fischer titration using a SI Analytics coulometer (Titroline 75 000 KFtrace) and the water content was 116–137 ppm for **1**–**5**, 88 and 92 ppm for **6** and **7**, respectively.

2.6. Thermal analysis

2.6.1. Thermogravimetric analysis (TGA)

The thermal stability of LevILs was investigated by thermal gravimetric analysis (TG) conducted in a TA Instruments Q500 TGA (weighing Precision ± 0.01%, sensitivity 0.1 μg, baseline dynamic drift < 50 μg). The temperature calibration was performed using curie point of nickel and Alumel standards and for mass calibration weight standards of 1 g, 500 mg, and 100 mg were used. All the standards were supplied by TA Instruments Inc. 12–15 mgs of each sample were heated in a platinum crucible as sample holder. First, the heating mode was set to isothermal at 60 °C in N_2 (80 cm^3/min) for 30 min. Then, the sample was heated from 40 °C to 500 °C at 10 °C min^{-1} under nitrogen (80 cm^3/min) and maintained at 600 °C for 3 min. Mass change was recorded as a function of temperature and time. TGA experiments were carried out in triplicate.

2.6.2. Differential scanning calorimetry (DSC)

The thermal behavior of LevILs was analyzed by a differential scanning calorimeter (TA DSC, Q250, USA, temperature accuracy ± 0.05 °C, temperature precision ± 0.008 °C, enthalpy precision ± 0.08%). Dry high purity N_2 gas with a flow rate of 50 cm^3/min was purged through the sample. 1–5 mg of each sample was loaded in pinhole hermetic aluminum crucibles and the phase behavior was explored under nitrogen atmosphere in the temperature range from −90 to 120 °C with a heating rate of 3, 5, 8, 10, and 12 °C/min. The temperature calibration was performed considering the heating rate dependence of the onset temperature of the melting peak of indium. The enthalpy was also calibrated using indium (melting enthalpy ΔH_m = 28.71 J g^{-1}). DSC experiments were carried out in duplicate. T_g was obtained by taking the midpoint of the heat capacity change on heating from a glass to a liquid. T_m was taken as the peak temperature of the endothermic peak on the heating run. The peak temperatures were chosen instead of the onset temperatures due to the complexity of the thermograms.

2.7. Viscosity

Viscosities of ILs as a function of temperature were measured using a Brookfield DV-II + Pro (Brookfield AMETEK, Inc., Middleboro, MA, USA) programmable viscometer, with an uncertainty of 2%. The measurements were carried out in the temperature range from 20 to 80 °C, controlled by a Brookfield TC-502 thermostat with an accuracy of 0.1 °C. Viscosity (η) was determined in the temperature range from 20 to 80 °C, applying 15 different shearing rates between 1 s^{-1} and 100 s^{-1}.

2.8. Density

Density was measured with 0.0001 g/cm^3 resolution and 0.001 g/cm^3 accuracy by use of a commercial density-meter (Anton Paar, DMA35 model). This instrument exploits a U-shaped oscillating tube as a sensing element. Measurements were collected at 10 different temperatures within the range ~17 °C – 21 °C.

2.9. Refractive index

A commercial prism-coupling refractometer (Metricon, 2010/M model) was employed for the determination of the refractive index with a standard error ± 0.0002. Described in detail elsewhere[48,49], this instrument utilizes a transparent reference prism that rests on a rotary table. The sample is attached to the base of the prism via a home-made liquid holder, forming an interface which is illuminated by either one out of five available laser sources emitting monochromatic radiation at 450 nm, 532 nm, 632.8 nm, 964 nm and 1551 nm. Measuring the reflectance at the prism/liquid interface for variable incidence angles, the phenomenon of total internal reflection (TIR) is observed, yielding the refractive index of the sample via the well-know TIR condition. Temperature is controlled via a thermal resistor that is properly inserted to heat the interface.

3. Results and discussion

3.1. Synthesis of levulinate ionic liquids (LevILs)

Two main synthetic strategies were undertaken to prepare the seven structurally-related levulinate ILs (LevILs Scheme 1). Both synthetic routes make use of ionic liquids as precursors and lead to the target LevILs through a metathesis reaction.

The imidazolium and phosphonium LevILs as well as the ammonium systems with long-chain alkyl substituents (**1**, **2**, **6** and **7**), were prepared from the commercially available methylcarbonate precursors following known procedures. This entailed a simple reaction with an equimolar amounts of the acid of interest (levulinic acid in the present case). The advantages of this synthetic method have been widely discussed in our previous work,[46,50] which allows for the preparation of LevILs in an operationally simple procedure and in high purity. In the case of the pyrrolidinium and piperidinium ILs, where the correspond-

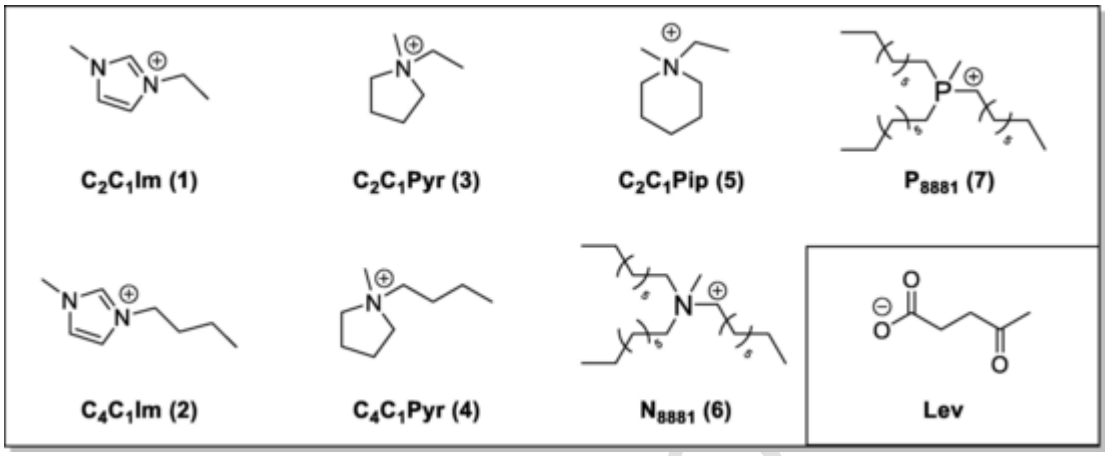

Scheme 1. Levulinate ionic liquids (LevILs) studied in the present work.

ing methyl carbonate precursors are not commercially available, the traditional metathesis processes were followed.[51] Among the possible well-known literature options,[47] the ion exchange resin technique was selected to avoid contamination with metals which could affect the physico-chemical properties of LevILs. Indeed, preliminary attempts with silver salts showed a possible interaction between the levulinate anion and the metal. Therefore, LevILs **3**–**5** were synthesized using an ion exchange resin starting from their bromide precursors, whose synthesis is reported in the supporting information. The chemical structures of LevILs (**1**–**7**) were assessed by NMR experiments (^{1}H and ^{13}C) while the absence of bromide anions was determined by means of the silver nitrate test. Particular care was devoted to the removal of water as it strongly affects the outcome of the forthcoming tests. For this reason, all samples were heated at 60 °C under high vacuum for 12 h before each measurement and the water content of LevILs was estimated by Karl Fischer titration.

3.2. Thermal analysis

Diffierential scanning calorimetry (DSC) and thermogravimetric analysis were carried out to ascertain the operative range of the synthesized LevILs. The thermal behaviour of the synthesised LevILs was investigated by DSC within the temperature range of −90 °C to 200 °C at different scannig rates (3, 5, 8, 10, 12 °C/min). Only [C_4C_1Pyr]Lev (4) showed clear phase transitions, with melting (T_m) and crystallization (T_c) at 41.6 °C (T_{peak}), 27.3 °C (T_{onset}) and −25.4 °C (T_{onset}), −33.3 °C (T_{peak}) respectively (Fig. 1a), and a glass trasition only in the first run. For this compound, the ratio between the glass transition and the melting temperature is in accord with the semiempirical rule of T_g / T_m = 2/3.[52] The T_c and T_m temperatures were estimated on the onset point and peak temperatures while T_g using the midpoint of transition. The rather broad difference between crystallization and melting event of **4** leads to a subcooled liquid at room temperature. All the other LevILs investigated showed a tendency to form glassy structures with glass transition temperatures (T_g) ranging between −60.9 °C and −80.6 °C. Fig. 1b shows the DSC thermogram of [C_2C_1Im]Lev (1) as a

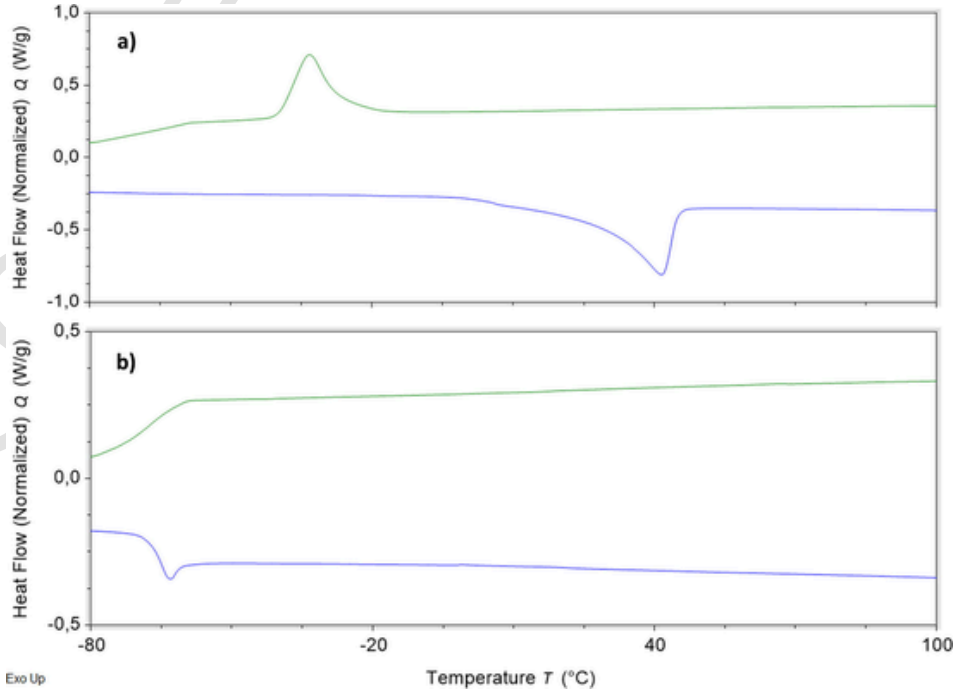

Fig. 1. Differential scanning calorimetry at 10 °C/min scanning rate of compound a) **[C_4C_1Pyr] Lev (4)** and b) **[C_2C_1Im] Lev (1).**

representative example of a typical thermoghraph observed for LevILs. The DSC curves of the other LevILs are reported in the supporting information (Figure S7-S13). The T_g values obtained from the different LevILs are reported in Table 1. Compounds **6** and **7** show very low values of T_g, a result which is attributable to the asymmetric structure of the cation and to the long alkyl chains that create a disordered structures with a consequent lowering of the T_g. While this latter effect explains the T_g values of bulky cations, for imidazolium, pyrrolidinium and piperidinium LevILs the differences between T_g values can be ascribed to the chemical nature of the cation and follow the order: $[C_2C_1Pyr]$Lev (3) < $[C_2C_1Im]$Lev (1) < $[C_2C_1Pyp]$Lev (5). The elongation of the alkyl chain from C2 to C4 in the pyrrolidinium series caused a marked variation in the thermal behavior of $[C_4C_1Pyr]$Lev (4) when compared to $[C_2C_1Pyr]$Lev (3). Conversely, for imidazolium ILs, no significant difference in the glass transition temperatures were observed for the same structural change.

A comparison with similar structures shows that $[C_4C_1Pyr]$Lev (4) displays a lower T_m than the corresponding acetate IL (T_m = 60 °C, value of temperature at signal peak[53]). Similarly, imidazolium LevIL **2** shows a lower T_g value than $[C_4C_1Im]$OAc.[53] Formate $[C_2C_1Im]$ exhibited a melting phenomenon at 52 °C,[54] while the analogous cation paired with the levulinate anion (LevIL **1**) displays only a glass transition.

Finally, the effect of the scanning rate on thermal behaviour was evaluated for all compounds. As known, crystallizations and glass transitions, being purely kinetic events, are strongly influenced by the scanning rate while the thermodinamically characterised melting events remain unchanged.[55] For this reason, faster scanning rates lead to an increase of the T_g for glassy forming LevILs while **4** showed a decrease of its T_c. Both phenomena vary linearly with the scanning rate. Therefore, it was possible to extrapolate the T_g and T_c value at 0 °C/min for all investigated LevILs (Figure S14-S15). The obtained values are reported in Table S1.

In parallel to the thermal behavior, the thermal stability of the synthesized LevILs was ascertained by thermogravimetric analysis (TGA). The analysis was performed at 10 °C/min up to 500 °C after a drying step. Nevertheless, almost all samples presented a mass loss event around 100 °C ascribable to the release of water, absorbed due to the LevILs' hygroscopic nature. The comparison of the TG and DTG curves is presented in Fig. 2, while the single thermograms of LevILs are reported in the Supplemetary File (Figure S16-S22). The values of the three characteristic parameters T_{start}, T_{onset} and T_{peak} obtained from the thermograms are summarized in Table 1. As reported in our previous work,[46] $[N_{8881}]$Lev (6) with a T_{onset} of 166.1 °C was the least stable LevIL, while $[P_{8881}]$Lev (7) (T_{onset} = 266.9 °C) was the most stable one of the series. Imidazolium LevILs showed a T_{onset} of 231.2 and 222.3 °C for $[C_2C_1Im]$Lev (1) and $[C_4C_1Im]$Lev (2), respectively. The same trend has been already observed for long chain fatty acid ILs featuring the same cations.[50] The newly synthesized piperidinium and the two pyrrolidinium levulinate ILs showed higher thermal stability compared to $[N_{8881}]$Lev (6) but lower T_{onset} than all the other investigated LevILs. Finally, the thermal stability of the LevILs with cations of various nature but substituted with the same alkyl chains (C2 and C1) followed this order: $[C_2C_1Pyr]$Lev (3) < $[C_2C_1Pip]$Lev (5) < $[C_2C_1Im]$Lev (1). According to the thermal stability classification of ILs proposed by Cao and Mu,[56] $[P_{8881}]$Lev (7) belongs to the "less stable" class (250 °C < T_{onset} < 300 °C), the imidazolium ILs belong to the "least stable" class (200 °C < T_{onset} < 250 °C), while ILs **3**, **4**, **5** and **6** are below the lower limit considered. Furthermore, small variations of the alkyl chain length on the same cation type (compare imidazolium **1** and **2** as well as pyrrolidinium **3** and **4**) seem to play a limited role in the thermal stability. Generally, LevILs show slightly higher stability than their respective acetate ILs analogues.[53,56,57] Furthermore, $[C_2C_1Im]$Lev displays a slightly higher T_{onset} value when compared to the formate [54] and other carboxylate analogues characterised by carbon chains of various length.[50,57] On the contrary, $[N_{8881}]$Lev (6) and $[P_{8881}]$Lev (7) present lower thermal stability than the respective long chain fatty acid ILs.[50].

Based on the DSC and TGA data, the operative liquid range for the proposed LevILs could be assessed and the results are summarized in Fig. 3. For $[C_4C_1Pyr]$Lev (4) the T_m was considered as the lower limit, while the T_g was used for all the other LevILs. The T_{onset} of the main degradation step was selected as the upper limit. It is clear that $[P_{8881}]$Lev (7) exhibits the widest liquid range among the investigated LevILs,

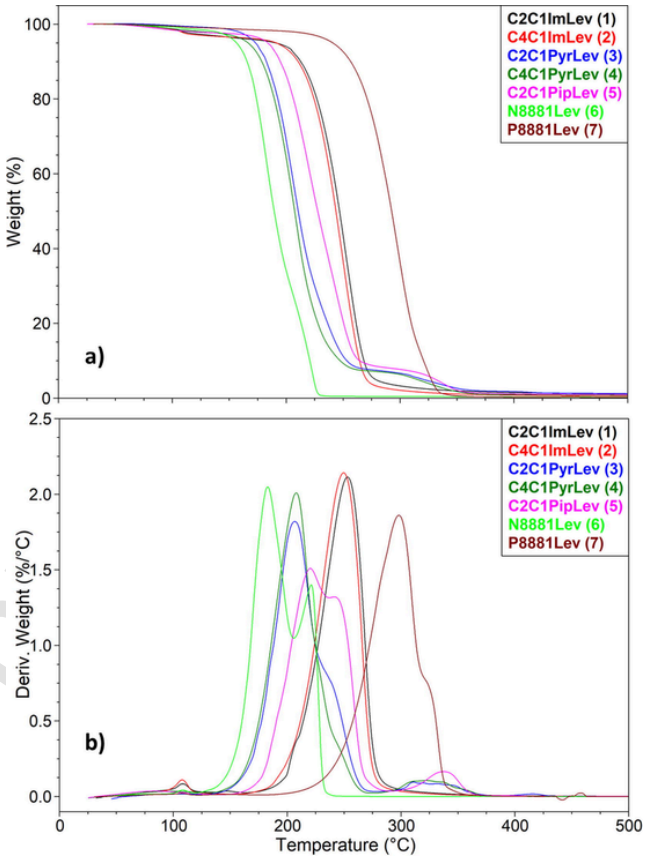

Fig. 2. TG (a) and DTG (b) of LevILs.

Table 1
Glass transition temperature (T_g), melting temperature (T_m), crystallization temperature (T_c) measured at 10 °C/min scanning rate and T_{start}, T_{onset}, and T_{peak} measured at heating rate of 10 °C/min of the investigated LevILs.

LevIL	DSC			TGA		
	T_g (°C)	T_m (°C) (ΔH_m (KJ/mol))	T_c (°C) (ΔH_c (KJ/mol))	T_{start} (5%) (°C)	T_{onset} (°C)	T_{peak} (°C)
$[C_2C_1Im]$ Lev (1)	−66.1	–	–	217.0	231.2	259.2
$[C_4C_1Im]$ Lev (2)	−65.9	–	–	208.1	222.3	249.6
$[C_2C_1Pyr]$ Lev (3)	−77.5	–	–	173.2	184.0	206.7
$[C_4C_1Pyr]$ Lev (4)	–	T_{peak} 41.6 T_{onset} 27.3 (11.39)	T_{peak} −33.3 T_{onset} −25.4 (11.32)	166.6	184.2	208.0
$[C_2C_1Pip]$ Lev (5)	−60.9	–	–	191.5	196.3	220.3
$[N_{8881}]$Lev (6)	−76.4	–	–	156.5	166.1	182.9
$[P_{8881}]$Lev r(7)	−80.6	–	–	241.3	266.9	298.2

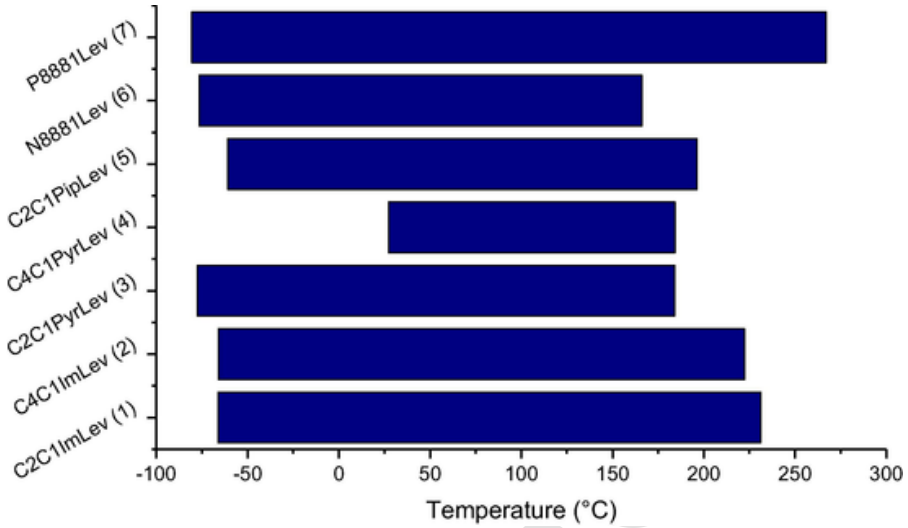

Fig. 3. Operative liquid range of LevILs.

followed by the imidazolium ILs. On the other hand, [C_4C_1Pyr]Lev (4) shows the narrowest liquid range, as a consequence of its melting point being above room temperature. Finally, the piperidinium IL (5) exhibits a similar liquid range to its pyrrolidinium analog **3** with a slight shift towards higher temperatures.

3.3. Viscosity

The viscosity of ILs is an important parameter which contributes to the transport properties and can be used to select the field of application. ILs' viscosity depends from the chemical nature of the cation and the anion, the temperature and the water content. For this reason, the study of viscosity in relation to the structural features of the LevILs cation is fundamental for a complete characterization of this class of compounds. The viscosity of the pure investigated LevILs is reported in Table S2. All LevILs show a Newtonian behaviour for shear rate range between 1 s^{-1} and 100 s^{-1} over the entire temperature range studied. As generally observed for ILs, the viscosity rapidly decreases on increasing the temperature and the relative viscosity differences were maintained throughout the temperature range studied (Fig. 4). From a comparison of the viscosities at 20 °C, the bulky ammonium ILs are characterized by a higher viscosity than the other LevILs, and viscosity decreases in the following order: [N_{8881}]Lev (6) > [C_2C_1Pip]Lev (5) > [P_{8881}]Lev (7) > [C_4C_1Im]Lev (2) > [C_2C_1Im]Lev (1) > [C_4C_1Pyr]Lev (4) > [C_2C_1Pyr]Lev (3). It is worth noting that the viscosity of the pyrrolidinium ILs is the lowest of the whole series while the structurally related piperidinium IL shows a considerably higher viscosity.

Focusing on the cation type, the viscosity trend is different from that reported for the structurally-related Tf_2N ILs, where the bulky ammonium remains the most viscous while the imidazolium systems are less viscous than the pyrrolidinium ones.[58] Comparing instead literature data of IL examples with levulinate and acetate as anions is particularly interesting. For [C_2C_1Im]OAc the viscosity value of 162 mPa·s[59] at 25 °C is only slightly lower than 170 mPa·s observed for [C_2C_1Im]Lev (1). Conversely, the value of 485 mPa·s at 25 °C[60] of [C_4C_1Im]OAc is significantly higher than that measured for [C_4C_1Im]Lev (2) (267 mPa·s). A similar difference is found also for the pyrrolidinium

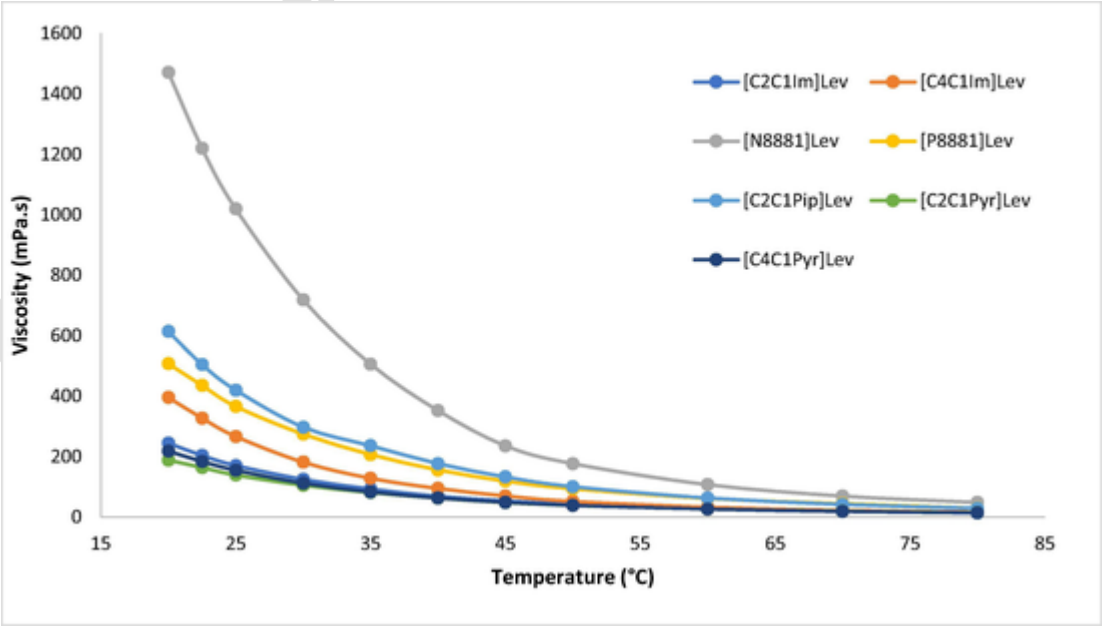

Fig. 4. Viscosity (mPa s) of LevILs as a function of temperature.

cation, even when substituted with the shortest side chain. Indeed, [C_2C_1Pyr]OAc and [C_2C_1Pyr]Lev (3) present viscosities of 240 and 139 mPa·s, respectively.

3.4. Fragility index

Glass-forming liquids are usually classified as "strong" or "fragile" depending on the trend of their viscosity with changing temperatures. Strong liquids are characterized by stable structures with a high degree of short range order, and exhibit only modest changes in properties during glass transition,[61-64] usually following an Arrhenius scaling of viscosity with temperature. On the contrary, fragile liquids have their properties dramatically altered in the glass transition range and are characterized by the lack of a consistent short range order.[65] The fragility index (*m*), defined as kinetic fragility when determined from viscosity measurements, is the most common parameter used to quantify the fragility of a glass-forming liquid and expresses the liquid dynamic rate of change upon cooling through the glass transition. In the description of the temperature dependence of viscosity, the Angell plot is the most commonly used scaling. According to this representation, the logarithm of viscosity is plotted as a function of the T_g-scaled inverse temperature (T_g/T),[61-64] with T as the absolute temperature and the glass transition temperature (T_g) defined as the temperature at which the liquid viscosity equals 10^{12} Pa•s. The slope of the Angell curve at T_g defines the fragility index (m). From the perspective of ionic liquids, T_g and m are parameters not only important in the definition of the rheological properties but are known to be also closely connected to the ionic mobility and the conductivity. As reported by Sippel *et al.*,[66] ILs that manifest both high fragility and low glass temperature are often characterized by low room-temperature resistivity. The investigation of ILs fragility appears therefore as an interesting approach for the design and development of ILs with both better viscous properties and enhanced ionic conductivity. The most widely used approaches reported in the literature for the calculation of *m* can be essentially divided between calorimetric ones[6768] (performed through flash or traditional DSC procedures) and viscosity-based ones,[69,70] though methods based on spectroscopic and dielectric measurements have also been proposed.[66,71] In this work, in order to better investigate the non-Arrhenius behavior manifested by the presented ILs, two different viscosity-based approaches (VFT and MYEGA models) have been considered and compared with the results obtained through DSC methodologies.

Although it is clear to the authors that the Arrhenius model equation (**Eq. (1)**) will not be sufficient for a good modelling of the viscosity-temperature relationship shown by ILs **1**–**7**, we still consider that a preliminary fitting with Eq. (1) can provide some valuable indication on the fragility of the considered ILs:

$$\ln(\eta) = \ln(\eta_\infty) + E_a/RT \quad (1)$$

where E_a is the activation energy for viscous flows and $\ln(\eta_\infty)$ is the viscosity at infinite temperature. High values of E_a indicate a hindered motion of the ions, mainly due to their size or to the presence of a strong network of interaction within the IL lattice. For glass-forming liquids, a good agreement between the experimental data and the Arrhenius model suggests a low entity modification of the physicochemical properties during the glass transition range, which in turn function as a preliminary assessment of their strength or fragility. The Arrhenius fitting results in Table 2, computed for ILs **1**–**7**, show a quite good agreement between the experimental data and the viscosity temperature relationship expressed by the Arrhenius model. This outcome provides good evidence for a strong liquid behavior in the case of all the ILs considered in the study.

On the other hand, although the data seem to fit well enough within the Arrhenius model to exclude a fragile behavior, it is also evident that this framework does not provide a fully satisfactory solution. For example, it can be indeed seen that a subtle but well perceivable deviation from linearity is present and therefore a better model is needed (Figure S23-S29).

The Vogel-Fulcher-Tammann (VFT) model is one of the most widely adopted for the description of glass-forming liquids.[69] The VFT equation appears similar to the Arrhenius one, but with a crucial difference in the (T-T_0) term:

$$\eta = \eta_\infty \exp[B/(T - T_0)] \quad (2)$$

with η_∞ representing the viscosity at infinite temperature and B and T_0 being fitting parameters related to the fragility index through the equation:

$$m = (B/T_g)/[(\ln 1_0)\left(1 - \frac{T_0}{T_g}\right)^2] \quad (3)$$

T_0, η_∞, B and m values obtained according to the VFT model through equations **(2) and (3)** are reported in Table 3.

Table 2
Arrhenius fitting parameters E_a and $\ln(\eta_\infty)$ obtained for ILs **1**–**7**.

	[C_2C_1Im] Lev (1)	[C_4C_1Im] Lev (2)	[C_2C_1Pyr] Lev (3)	[C_4C_1Pyr] Lev (4)	[C_2C_1Pip] Lev (5)	[N_{8881}] Lev (6)	[P_{8881}] Lev (7)
E_a (KJ/mol)	41.4792	46.3648	37.2630	39.7415	44.8674	50.4780	40.9139
$\ln(\eta_\infty)$	−11.617	−13.170	−10.125	−11.031	−12.049	−13.480	−10.616
η_∞	$9.01\bullet10^{-6}$	$1.91\bullet10^{-6}$	$4.01\bullet10^{-5}$	$1.62\bullet10^{-5}$	$5.85\bullet10^{-6}$	$1.40\bullet10^{-6}$	$2.45\bullet10^{-5}$
R^2	0.9946	0.9893	0.9929	0.9909	0.9982	0.9941	0.9968

Table 3
Fitting parameters B, η_0 and T_0, fragility index m and linearity deviation × obtained according to VFT model for ILs **1**–**7**.

	[C_2C_1Im] Lev (1)	[C_4C_1Im] Lev (2)	[C_2C_1Pyr] Lev (3)	[C_4C_1Pyr] Lev (4)	[C_2C_1Pip] Lev (5)	[N_{8881}] Lev (6)	[P_{8881}] Lev (7)
T_0(K)	182.65288	180.55721	159.64662	189.08466	178.72141	146.85834	138.50716
B	904.70302	1074.66442	1138.82637	797.41621	981.6227	1736.32873	1590.43435
m	161.98603	157.72042	75.26108	623.99254	94.62637	72.46674	47.27045
η_∞	0.06791	0.0285	0.03743	0.10296	0.11459	0.01042	0.01738
R^2	0.9999	0.9998	0.9996	0.9999	0.9990	0.9988	0.9998
x	0.1087	0.1201	0.1833	0.0527	0.1467	0.2331	0.2763

As highlighted in Figures S30-S36, the VFT model provides an excellent fitting for the collected experimental viscosity data, and the obtained parameters were therefore used to calculate the fragility index of the analyzed ILs and the non-linearity parameter *x*. However, the values of *m* reported in Table 3 appear to express a fragility level mismatching with the low non-linearity parameters obtained and also seem inconsistent with the results obtained from the Arrhenius fitting, suggesting a stronger liquid behavior. Exemplary is the case of [C_4C_1Pyr]Lev (4) where a very low × parameter is associated to an extremely high fragility index. The limitations of the VFT model are known and a generalized overestimation of the viscosity values at low temperatures, due to the mathematical divergence at $T = T_0$[72,73] is often described. From a physical point of view, the divergence at T_0 also represent a problem, implicitly setting the configurational entropy value of the system to zero at temperatures usually much higher than 0 K.[74].

More recently, another model overcoming these issues has been proposed by Mauro, Yue, Ellison, Gupta and Allan (MYEGA model),

$$log(\eta) = log(\eta_\infty) + [12 - -log(\eta_\infty)](T/T_g)\, exp\{[m/(12 - log(\eta_\infty))] - 1](T_g/T) - 1\} \quad (4)$$

with η_∞, T_g and *m* as fitting parameters representing the viscosity at infinite temperature, the glass transition temperature and the fragility index, respectively. The MYEGA model fitting parameters obtained for ILs **1**–**7** are reported in Table 4.

The MYEGA equation was found to fit well the experimental data (Figure S37-S43) and provided values for T_g very close to those obtained through calorimetric analysis. As shown in Table 4, the differences between predicted and experimental T_g are modest for all the considered ILs, exceeding 15 °C only for **5** (25.18 °C) while the best agreement is observable for **3**, **7** and **1** with differences of only 3.62 °C, 4.33 °C and 6.62 °C respectively. The fragility index values were also found to be more coherent with the expected strong liquid behavior than those obtained with the VFT model, resulting in the highest values of 67.21 and 65.31 calculated for **2** and **4** respectively. All the reported fragility indexes were found to fall within a narrow range of values, stretching from 39.05 (5) to 67.21 (2). In order to verify the reliability of the calculated *m* parameters, a calorimetric approach has also been followed. The variation of the T_g values as a function of the heating rate (β) provides a viable method for the calculation of the apparent activation energy (E_a) and of the fragility index (*m*).[68,75] By applying equations **(5) and (6)** (Figure S44), the activation energy and fragility indexes of ILs **1**–**7** have been calculated and reported in Table 5.

$$\frac{d\ln\beta}{d(\frac{1}{T_g})} = \frac{-E_a}{R} \quad (5)$$

$$m = \left(\frac{1}{2.303}\right) * \left[\frac{E_a(T_g)}{RT_g}\right] \quad (6)$$

where $\ln\beta$ is the logarithm of the heating rate, T_g is the glass transition temperature and E_a is the activation energy. The fragility index was calculated using the T_g extrapolated at 0 °C/min scan rate (Table S3).

From the reported data it appears that both DSC and MYEGA approaches estimate a similar level of fragility for all the considered ILs, even if, in few cases, the computed *m* values present clear discrepancies (like in the case of **6** and **3**). The lack of agreement of *m* values obtained through different methodologies has also been reported by Tao *et al.* [67], who also proposed a few possible causes for this phenomenon. A strong incoherence between the calculated values, however, is only observable for compound **7**, where the DSC method points toward a much more fragile behavior than the one indicated by the MYEGA model. Despite these limitations, the results obtained according to the MYEGA model are closer to the DSC-derived data than the fragility index values obtained through the VFT model, where a satisfactory agreement can be observed only for **3**. The MYEGA fitting of the experimental data was also performed by alternatively using the T_g and the *m* parameter values obtained with other techniques (Table S4). The fit resulted improved for **1**, **2** and **6**, and remarkable results were obtained especially for **5** (m from 39.04 to 59.79 and T_g from 184.25 K to 202.04 K).

3.5. Density

Density and its temperature dependence, quantified via the thermal expansion coefficient, are key thermophysical properties that are needed in all kind of industrial applications as well as for the development of equations of state and predictive tools. We measured the densities of the ionic liquids under investigation at several temperatures between 17 °C and 21 °C. Then, experimental data were fitted to the following equation:

$$\rho_T = \frac{\rho_{20°C}}{1 + \beta_{20°C}.(T - 20°C)}\ , \quad (7)$$

Table 4
Fitting parameters η_∞, T_g and fragility index *m* obtained according to MYEGA model for ILs **1**–**7**. T_g DSC values reported have been extrapolated at 0 °C/min scan rate from DSC data.

	[C_2C_1Im] Lev (1)	[C_4C_1Im] Lev (2)	[C_2C_1Pyr] Lev (3)	[C_4C_1Pyr] Lev (4)	[C_2C_1Pip] Lev (5)	[N_{8881}] Lev (6)	[P_{8881}] Lev (7)
T_g (K)	198.32553	215.55636	199.10485	207.77260	184.25504	205.98482	187.06382
m	54.10487	67.20859	58.67679	65.31150	39.04690	49.13952	42.98131
η_∞	0.32470	0.98523	0.77343	1.05631	0.05247	0.34312	0.18730
R^2	0.9999	0.9995	0.9994	0.9999	0.9995	0.9984	0.9994
T_g DSC (K)	204.949	205.199	195.489	199.610	209.439	191.498	191.390

Table 5
Activation energy (E_a) and fragility indexes (*m*) calculated at 10 °C/min scan rate and extrapolated to 0 °C/min of ILs **1**–**7**. Fragility indexes (*m*) calculated through MYEGA and VFT model are also reported for comparison.

	[C_2C_1Im]Lev (1)	[C_4C_1Im]Lev (2)	[C_2C_1Pyr]Lev (3)	[C_4C_1Pyr]Lev (4)	[C_2C_1Pip] Lev (5)	[N_{8881}] Lev (6)	[P_{8881}] Lev (7)
E_a (KJ/mol)	258.24	255.65	307.21	/	210.93	102.69	404.38
m (0 °C/min)	65.81	65.07	82.07	/	52.60	28.01	110.35
m MYEGA	54.10487	67.20859	58.67679	65.31150	39.04690	49.13952	42.98131
m VFT	161.98603	157.72042	75.26108	623.99254	94.62637	72.46674	47.27045

where ρ_T is density at temperature T, ρ(20 °C) is the density at the reference temperature of 20 °C and β(20 °C) is the thermal expansion coefficient at the same temperature, defined as.

$$\beta_{20°C} = -\frac{1}{\rho_{20°C}} \cdot \frac{\partial \rho}{\partial T}. \quad (8)$$

Fit parameters and corresponding R-squared values are tabulated in Table 6.

We observed that room temperature densities were close to unity and decreased in the order $[C_2C_1Im]$Lev (1) > $[C_2C_1Pip]$Lev (5) > $[C_2C_1Pyr]$Lev r(3) > $[C_4C_1Im]$Lev (2) > $[C_4C_1Pyr]$Lev (4) > $[P_{8881}]$Lev (7) > $[N_{8881}]$Lev (6). The thermal expansion coefficient is on the high side among common families of ionic liquids[76] and still low compared to ordinary organic solvents, such as methanol, acetone and benzene.

3.6. Refractive index

3.6.1. Experimental results and modelling

The refractive index of the seven ionic liquids was determined as a function of temperature at five different wavelengths within the visible and near-infrared range (450 nm, 532 nm, 632.8 nm, 964 nm and 1551 nm). During the experimental procedure, the sample was not kept in an airtight container and, in order to avoid water reabsorption from the atmosphere, our measurements were restricted to elevated temperature only (typically, between 80 °C and 130 °C in steps of 5 °C). Data were fitted to the following Sellmeier equation, which captures simultaneously wavelength (λ) and temperature (T) dependencies:

$$n(\lambda, T) = \left[1 + \frac{s(T) \bullet \lambda^2}{\lambda^2 - \lambda_{uv}^2} + d \bullet \lambda^2\right]^{1/2} \quad (9)$$

Coefficient λ_{uv} represents the nearby absorption peak in the ultraviolet, $s(T)$ is the corresponding resonance strength and d is an additional fit parameter introduced to adjust the refractive index fit towards the longer infrared wavelengths. In agreement with observations reported in previous studies, [77,78] we concluded that it is sufficient to incorporate the temperature dependence into the resonance strength, according to.

$$s(T) = s_1 + s_2 \bullet T, \quad (10)$$

while keeping λ_{uv} and d constant. Calculated values of the Sellmeier coefficients for the seven ionic liquids are summarised in Table 7. The corresponding R-squared values exceed 0.998, indicating an excellent fit quality (typically, the Sellmeier equation reproduces experimental data within ± 0.0002, which is comparable to experimental accuracy).

The Sellmeier equation is known not to be reliable outside the spectral range of measurement (450–1551 nm). On the contrary, due to the simple linear scaling of the refractive index with temperature, it can be safely assumed that Eq. (9) produces accurate estimates within the entire liquid phase, including room temperature. To that end, Table 8 presents extrapolated values of the refractive index at 20 °C.

Fig. 5a depicts the wavelength dependence of the refractive index at several selected temperatures for $[C_2C_1Pip]$Lev (5). Fig. 5b shows instead the temperature dependence of the refractive index of $[C_4C_1Im]$Lev (2) at the five chosen wavelengths. In these indicative plots, we clearly observe normal chromatic and temperature dispersion; in other words, the refractive index decreases as wavelength/temperature increases. This behaviour is shared by all ionic liquids under investigation. Temperature dispersion can be quantified via the derivativedn/dT, which is commonly referred to as the thermooptic coefficient. Differentiating the Sellmeier equation yields.

$$\frac{dn}{dT} = \frac{s_2}{2n(\lambda.T)} \bullet \frac{\lambda^2}{\lambda^2 - \lambda_{uv}^2}. \quad (11)$$

Similarly, chromatic dispersions can be expressed in terms of (i) the group index n_g that regulates the group velocity$u_g(= c/n_g)$, which is the propagation velocity of the wavepacket envelope containing the spectral components of a polychromatic beam travelling through a dispersive medium and (ii) the dispersion of group velocityβ_2. By definition, it is.

$$\begin{aligned} n_g &= \frac{c}{u_g} \\ &= n - \lambda \bullet \frac{dn}{d\lambda} \quad \text{and} \quad \beta_2 \\ &= \frac{\lambda^3}{2\pi c^2} \bullet \frac{d}{d\lambda}\left(\frac{dn}{d\lambda}\right), \end{aligned} \quad (12)$$

where differentiation of the Sellmeier equation yields.

$$\frac{dn}{d\lambda} = \frac{\lambda}{n(\lambda.T)} \bullet \left[d - \frac{s(T) \bullet \lambda_{uv}^2}{\left(\lambda^2 - \lambda_{uv}^2\right)^2}\right]. \quad (13)$$

The thermooptic coefficient, the group index and the group velocity dispersion all exhibit wavelength and (weaker) temperature dependencies. Calculated according to Eq. (11), these dependencies are shown in Fig. 6 fordn/dT. Exemplary values for the room temperature n_g and β_2 at two different wavelengths (namely, 500 nm in the visible and 1000 nm

Table 6
Density and thermal expansion coefficient extrapolated from data fits to Eq. (7), along with corresponding R-squared values.

	ρ(20 °C) (g/cm^3)	β(20 °C) × 10^4 ($°C^{(-1)}$)	R^2
$[C_2C_1Im]$Lev (1)	1.12291	8.65216	0.994
$[C_4C_1Im]$Lev (2)	1.08631	8.08084	0.994
$[C_2C_1Pyr]$Lev (3)	1.10450	7.66872	0.997
$[C_4C_1Pyr]$Lev (4)	1.06835	7.53310	0.987
$[C_2C_1Pip]$Lev (5)	1.10502	7.42149	0.994
$[N_{8881}]$Lev (6)	0.92295	8.98824	0.997
$[P_{8881}]$Lev (7)	0.92958	10.12016	0.993

Table 7
Sellmeier coefficients for the seven ionic liquids, according to Eqs. (8) and (9). R-squared is also shown.

	s_1	s_2 ($°C^{(-1)}$)	$\lambda_{uv}(\mu m)$	$d(\mu m^{-2})$	R^2
$[C_2C_1Im]$Lev (1)	1.21464405	−0.000728108	0.117532272	−0.000681503	0.9996
$[C_4C_1Im]$Lev (2)	1.193888519	−0.000728395	0.11544471	−0.000424713	0.9996
$[C_2C_1Pyr]$Lev (3)	1.191659204	−0.000768017	0.104705819	−0.001164869	0.9997
$[C_4C_1Pyr]$Lev (4)	1.181294539	−0.000779386	0.105319457	−0.00096703	0.9984
$[C_2C_1Pip]$Lev (5)	1.207356868	−0.000758323	0.106461112	−0.000703452	0.9992
$[N_{8881}]$Lev (6)	1.125556841	−0.000774146	0.105240374	0.000277913	0.9987
$[P_{8881}]$Lev (7)	1.148837184	−0.000850205	0.109873217	0.000262521	0.9983

Table 8
Extrapolated refractive indices for the five wavelengths of measurement at 20 °C.

	450 nm	532 nm	632.8 nm	964 nm	1551 nm
$[C_2C_1Im]$Lev (1)	1.5125	1.5038	1.4976	1.4891	1.4851
$[C_4C_1Im]$Lev (2)	1.5041	1.4958	1.4899	1.4819	1.4781
$[C_2C_1Pyr]$Lev (3)	1.4978	1.4911	1.4863	1.4796	1.4761
$[C_4C_1Pyr]$Lev (4)	1.4943	1.4876	1.4827	1.4761	1.4727
$[C_2C_1Pip]$Lev (5)	1.5042	1.4972	1.4922	1.4853	1.4819
$[N_{8881}]$Lev (6)	1.4746	1.4681	1.4635	1.4573	1.4546
$[P_{8881}]$Lev (7)	1.4845	1.4773	1.4721	1.4653	1.4622

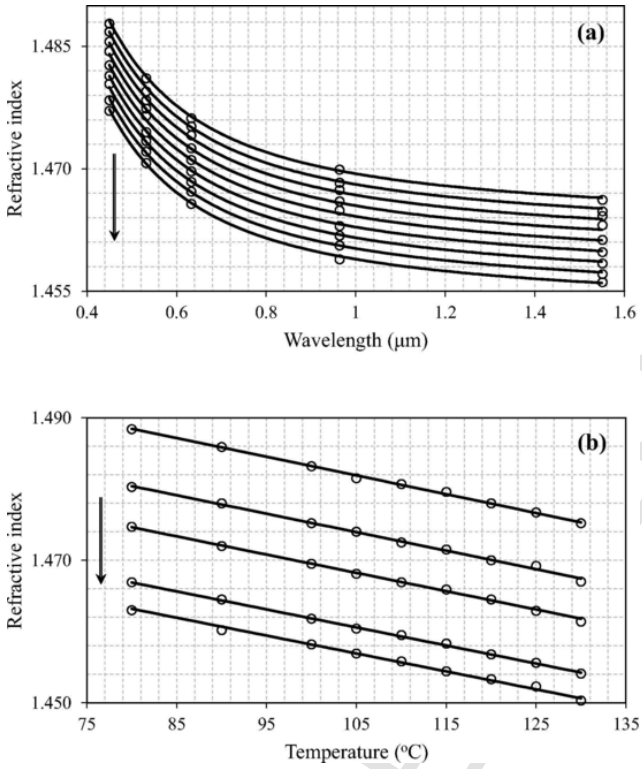

Fig. 5. (a) Refractive index of $[C_2C_1Pip]$Lev (5) as a function of wavelength at nine different temperatures from 80 °C to 120 °C in steps of 5 °C. (b) Refractive index of $[C_4C_1Im]$Lev (2) as a function of temperature at the five wavelengths of measurement (450 nm, 532 nm, 632.8 nm, 964 nm and 1551 nm) Open circles: experimental data. Solid lines: Sellmeier fits. Arrow indicates direction of increasing temperature (a) and wavelength (b), respectively.

in the near infrared) are tabulated in the first two columns of Table 9. These calculations follow the substitution of Eq. (13) into Eq. (12).

Dictating light propagation and interfacial phenomena, knowledge of the refractive and dispersive properties of ionic liquids are key for the design of novel photonic devices within the rapidly expanding field of optofluidics. To this end, ionic liquids have been used in wave guiding, beam focusing and laser development applications.[79-83] The optical constants are also highly relevant for understanding the interactions between ionic liquids and electromagnetic radiations at ultrashort timescales.[84-87] Furthermore, the refractive and dispersive constants are directly related to the molecular structure of liquids and are connected to various other physicochemical properties. At a more fundamental level, the refractive index yields the electronic polarizability α_e according to the Lorentz-Lorenz law.

$$\alpha_e = \frac{3}{4\pi} \bullet \frac{M}{\rho N_\alpha} \bullet \frac{n^2-1}{n^2+2} \tag{14}$$

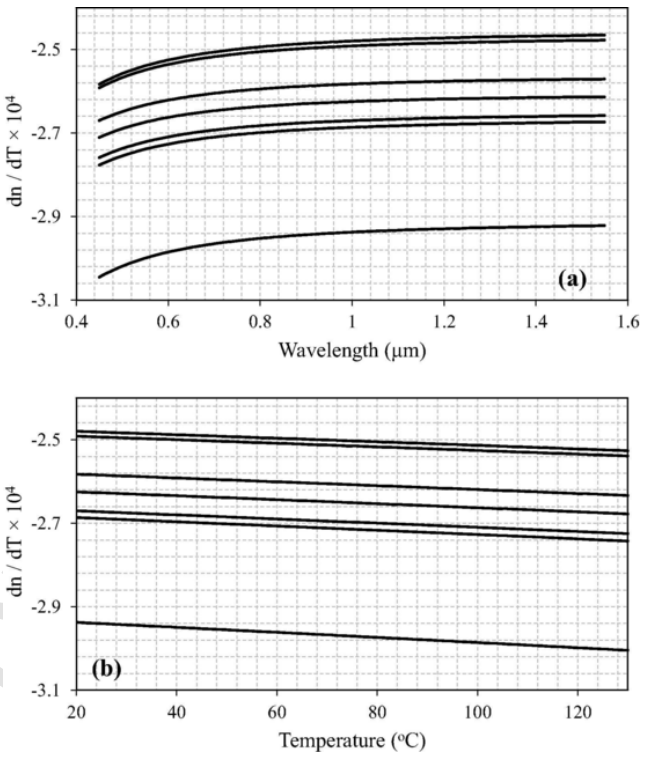

Fig. 6. (a) Thermooptic coefficient of the seven ionic liquids as a function of wavelength and constant temperature (20 °C). (b) Thermooptic coefficient of the seven ionic liquids as a function of temperature and constant wavelength (1000 nm). Calculations are based on Eq. (13). In both plots, dn/dT decreases in the cation order $[C_2C_1Im]$Lev (1) > $[C_4C_1Im]$Lev (2) > $[C_2C_1Pip]$Lev (5) > $[C_2C_1Pyr]$Lev (3) > $[C_4C_1Pyr]$Lev (4) > $[N_{8881}]$Lev (6) > $[P_{8881}]$Lev (7).

Table 9
Dispersion parameters ^{n_g} andβ_2, electronic polarizability a_e and its temperature coefficient Φ at 20 °C. Calculations assume a visible ($\lambda_1 = 500nm$) and an infrared ($\lambda_2 = 1000nm$) wavelength.

	^{n_g}		$\beta_2(fs^2/mm)$		$a_e(Å^3)$		$\Phi \times 10^4$ ($°C^{(-1)}$)	
	λ_1	λ_2	λ_1	λ_2	λ_1	λ_2	λ_1	λ_2
$[C_2C_1Im]$Lev (1)	1.556	1.501	139.7	61.0	23.8	23.0	4.4	4.3
$[C_4C_1Im]$Lev r (2)	1.545	1.493	132.3	58.3	27.2	26.4	3.7	3.7
$[C_2C_1Pyr]$Lev (3)	1.531	1.489	105.5	46.5	23.9	23.4	3.0	3.0
$[C_4C_1Pyr]$Lev (4)	1.528	1.485	106.2	47.0	27.6	26.9	2.8	2.7
$[C_2C_1Pip]$Lev (5)	1.539	1.495	110.7	49.3	25.7	25.0	2.9	2.9
$[N_{8881}]$Lev (6)	1.507	1.465	102.5	46.8	58.0	56.6	4.0	3.9
$[P_{8881}]$Lev (7)	1.520	1.474	114.7	51.8	60.5	58.9	4.7	4.7

where ε_o is the permittivity of free space, N_α is Avogadro's number and M is the molar mass. Differentiating the Lorentz-Lorenz law leads to the following expression for the temperature coefficient Φ of electronic polarizability:

$$\Phi = \frac{1}{\alpha_e} \bullet \frac{d\alpha_e}{dT} = \beta + \frac{6n}{(n^2-1)(n^2+2)} \bullet \frac{dn}{dT} \tag{15}$$

All parameters in Eqs. (14) and (15) are known for the ionic liquids under investigation (including density ρ and thermal expansion coefficient β at 20 °C). Hence, values of the electronic polarizability and its

temperature coefficient can be straightforwardly calculated as a function of wavelength at room temperature. The last two columns in Table 9 present such exemplary calculations at 500 nm and 1000 nm.

3.6.2. Further insights and phenomenological observations

The refractive index decreases consistently in the order $[C_2C_1Im]$Lev (1) > $[C_2C_1Pip]$Lev (5) > $[C_4C_1Im]$Lev (2) > $[C_2C_1Pyr]$Lev (3) > $[C_4C_1Pyr]$Lev (4) > $[P_{8881}]$Lev (7) > $[N_{8881}]$Lev (6) (see, for example, Table 8). Unsurprisingly, if the mutual transposition between $[C_4C_1Im]$Lev (2) and $[C_2C_1Pyr]$Lev (3) is disregarded, this is the also the order in which density decreases. The clear trend of refractive index increase with increasing density is depicted in Fig. 7. The refractive index span (1.512 to 1.463 in the visible range at room temperature) is consistent with values previously reported for imidazolium ILs,[48,77,78] as well as for several solvents with high refractive index such as benzene, toluene and carbon tetrachloride.[49].

The thermooptic coefficient reduces in the order $[C_2C_1Im]$ Lev (1) > $[C_4C_1Im]$ Lev (2) > $[C_2C_1Pip]$ Lev (5) > $[C_2C_1Pyr]$Lev (3) > $[C_4C_1Pyr]$Lev (4) > $[N_{8881}]$Lev (6) > $[P_{8881}]$Lev (7), which mirrors the refractive index trend. The observed order is expected, since dn/dT is negative and inversely proportional to n according to Eq. (12). The pattern reverses, however, between $[C_4C_1Im]$Lev (2) and $[C_2C_1Pip]$ Lev (5), as well as between $[N_{8881}]$Lev (6) and $[P_{8881}]$Lev (7). This trend reversal can be ascribed to the corresponding value of the Sellmeier coefficients_2. The thermooptic coefficient is in the $2.5\bullet10^{(-4)}$ $°C^{(-1)}$ to $3.0\bullet10^{(-4)}$ $°C^{(-1)}$ range, which is compatible with the corresponding values obtained for imidazolium ILs[48,77,78] yet lower than the thermooptic coefficient estimates reported for benzene, toluene and carbon tetrachloride.[49].

The dispersion parameters $^{n}_{g}$ and β_2 decrease in the order $[C_2C_1Im]$ Lev (1) < $[C_4C_1Im]$Lev (2) < $[C_2C_1Pip]$Lev (5) < $[C_2C_1Pyr]$Lev (3) < $[C_4C_1Pyr]$Lev (4) < $[P_{8881}]$Lev (7) < $[N_{8881}]$Lev (6) and $[C_2C_1Im]$Lev (1) < $[C_4C_1Im]$Lev (2) < $[P_{8881}]$Lev (7) < $[C_2C_1Pip]$Lev (5) < $[C_4C_1Pyr]$Lev (4) < $[C_2C_1Pyr]$Lev (3) < $[N_{8881}]$Lev (6), respectively. Several trends may be identified, such as the similarity between the scaling of $^{n}_{g}$ and the thermooptic coefficient with cation. This observation may be related to the fact that both quantities result from first order derivatives of the refractive index (with respect to wavelength and temperature, respectively). Regardless, values of $^{n}_{g}$ and β_2 (see Table 9) are comparable with those reported previously for imidazolium ILs[78] and various common solvents.[49].

The electronic polarizability is in the range of $25Å^3$ for all ionic liquids under investigation, with the exception of $[N_{8881}]$Lev (6) and $[P_{8881}]$Lev (7). These two materials exhibit polarizabilities that are roughly double mainly due to their higher molar mass and lower density. The temperature coefficient Φ is positive and smaller, yet comparable to the thermal expansion coefficient. This behaviour is not typical of condensed matter, since Φ is generally two orders of magnitude smaller than the thermal expansion coefficient. Nevertheless, it has been observed experimentally with imidazolium ionic liquids[48] and is in accord with molecular dynamics simulations on pyridinium ionic liquids, which predict a substantial increase of dipole moment with increasing temperature.[88].

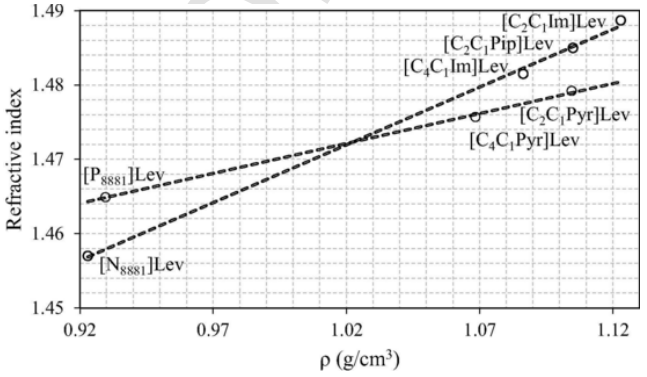

Fig. 7. Refractive index (λ = 1 μm,T = 20 °C) as a function of density (T = 20 °C) for the seven ionic liquids, as is indicated. The straight lines are inserted to guide the reader's eye.

4. Conclusions

A panel of physicochemical properties of seven levulinate-based ILs containing some of the most used cations has been experimentally determined and analyzed. All ILs displayed glass transitions only (T_g < −60 °C) with the exception of $[C_4C_1Pyr]$Lev (4), which presented melting at 41.6 °C (T_{peak}) and a crystallization at −33.3 °C (T_{peak}). This latter thermal behaviour is substantially different from that of $[C_2C_1Pyr]$Lev (3), which only showed a glass transition. Furthermore, the same C2–>C4 elongation of the alkyl chain did not determine the same change in the thermal behavior in the case of the imidazolium cation. In terms of thermal stability, the data obtained are in agreement with the usually observed order, with ammonium (6) and phosphonium (7) LevILs the least and most stable ILs of the series. Moreover, the thermal stability of the remaining LevILs decreased in the order $[C_2C_1Im]$ Lev (1) ≈ $[C_4C_1Im]$Lev (2) > $[C_2C_1Pip]$Lev (5) > $[C_2C_1Pyr]$Lev (3) ≈ $[C_4C_1Pyr]$Lev (4). LevILs showed a Newtonian behaviour in the investigated shearing rates range, with a marked reduction in the viscosity with increasing temperatures. $[N_{8881}]$Lev (6) resulted by far the most viscous IL at 20 °C. It is worth mentioning that $[C_4C_1Im]$Lev (2) and $[C_2C_1Pyr]$Lev (3) displayed lower viscosity values at 25 °C than the corresponding acetate ILs. The fragility index of the LevILs was evaluated applying the VFT and MYEGA viscosity-based models. The MYEGA model gave the most reliable data and highlighted the strong liquid nature of the LevILs. These findings were further corroborated through an alternative approach, based on the study of the glass transition temperature as a function of the heating rate for the determination of the fragility index. To the best of our knowledge, this is the first time that two complementary models have been applied to study a panel of ILs.

The density of the LevILs was found to vary in the vicinity of$1 g/cm^3$, while the thermal expansion coefficient was found to span a range (~8 $°C^{(-1)}$ to ~ 10 $°C^{(-1)}$) that is typical of many common solvents. The refractive index of the seven ILs was experimentally determined at five different wavelengths within the visible and near-infrared spectral range. At each wavelength, measurements were repeated at several temperatures between 80 °C and 130 °C. A single resonance Sellmeier equation was found to reproduce experimental data with sufficient accuracy, capturing simultaneously the wavelength and temperature dependence of the refractive index. Chromatic and temperature dispersion parameters ($dn/dT, n_g$ and β_2) were then evaluated, along with the electronic polarizability (a_e) and its temperature coefficient (Φ). Trends and correlations were identified, including the systematic refractive index increase with increasing density, as well as the refractive index scaling with cation, which follows consistently the order $[C_2C_1Im]$Lev (1) > $[C_2C_1Pip]$Lev (5) > $[C_4C_1Im]$Lev (2) > $[C_2C_1Pyr]$Lev (3) > $[C_4C_1Pyr]$Lev (4) > $[P_{8881}]$Lev (7) > $[N_{8881}]$Lev (6).

Overall, the presented analysis highlights the suitability of these ILs for future applications where other carboxylate ILs have been already explored. Furthermore the concept of ILs as designers' materials is confirmed in the present case, where variations of physicochemical properties have been observed as a consequence of subtle structural variations within the cationic moiety. Indeed, the in-depth knowledge of this interplay is a fundamental requirement for selecting the best LevIL for the application of interest.

Declaration of Competing Interest

The authors declare that they have no known competing financial interests or personal relationships that could have appeared to influence the work reported in this paper.

Appendix A. Supplementary data

Supplementary data to this article can be found online at https://doi.org/10.1016/j.molliq.2022.118850.

References

[1] T. Welton, Ionic liquids: a brief history, Biophys. Rev. 10 (3) (2018) 691–706, https://doi.org/10.1007/s12551-018-0419-2.

[2] S.K. Singh, A.W. Savoy, Ionic liquids synthesis and applications: An overview, J. Mol. Liq. 297 (2020) 112038, https://doi.org/10.1016/j.molliq.2019.112038.

[3] M.E. Di Pietro, F. Castiglione, A. Mele, Polar/apolar domains' dynamics in alkylimidazolium ionic liquids unveiled by the dual receiver NMR 1H and 19F relaxation experiment, J. Mol. Liq. 322 (2021) 114567, https://doi.org/10.1016/j.molliq.2020.114567.

[4] M.E. Di Pietro, F. Castiglione, A. Mele, Anions as dynamic probes for ionic liquid mixtures, J. Phys. Chem. B. 124 (14) (2020) 2879–2891, https://doi.org/10.1021/acs.jpcb.0c0002610.1021/acs.jpcb.0c00026.s001.

[5] A. Cimini, O. Palumbo, E. Simonetti, M. De Francesco, G.B. Appetecchi, S. Fantini, R. Lin, A. Falgayrat, A. Paolone, Decomposition temperatures and vapour pressures of selected ionic liquids for electrochemical applications, J. Therm. Anal. Calorim. 142 (5) (2020) 1791–1797, https://doi.org/10.1007/s10973-020-10334-5.

[6] S. Murugesan, O.A. Quintero, B.P. Chou, P. Xiao, K. Park, J.W. Hall, R.A. Jones, G. Henkelman, J.B. Goodenough, K.J. Stevenson, Wide electrochemical window ionic salt for use in electropositive metal electrodeposition and solid state Li-ion batteries, J. Mater. Chem. A. 2 (7) (2014) 2194–2201, https://doi.org/10.1039/C3TA15010K.

[7] B. Wang, L.i. Qin, T. Mu, Z. Xue, G. Gao, Are ionic liquids chemically stable? Chem. Rev. 117 (10) (2017) 7113–7131, https://doi.org/10.1021/acs.chemrev.6b00594.

[8] M. Boumediene, B. Haddad, A. Paolone, M. Drai, D. Villemin, M. Rahmouni, S. Bresson, O. Abbas, Synthesis, thermal stability, vibrational spectra and conformational studies of novel dicationic meta-xylyl linked bis-1-methylimidazolium ionic liquids, J. Mol. Struct. 1186 (2019) 68–79, https://doi.org/10.1016/j.molstruc.2019.03.019.

[9] S. Muhammad, F.I. Ali, M.N. Javed, A.A. Wasim, A. Bari, F. Rafique, M.A. Ilyas, K. Riaz, S.J. Mahmood, A. Ahmed, I.A. Hashmi, Effect of supramolecular polymeric aggregation in room temperature ionic liquids (RTILs) on catalytic activity in the synthesis of 4H-chromene derivatives and Knoevenagel condensation, J. Mol. Liq. 322 (2021) 114503, https://doi.org/10.1016/j.molliq.2020.114503.

[10] S.T. Keaveney, R.S. Haines, J.B. Harper, Ionic liquid solvents: the importance of microscopic interactions in predicting organic reaction outcomes, Pure Appl. Chem. 89 (2017) 745–757, https://doi.org/10.1515/pac-2016-1008.

[11] M.J. Trujillo-Rodríguez, H.e. Nan, M. Varona, M.N. Emaus, I.D. Souza, J.L. Anderson, Advances of ionic liquids in analytical chemistry, Anal. Chem. 91 (1) (2019) 505–531, https://doi.org/10.1021/acs.analchem.8b04710.

[12] D.J.S. Patinha, H. Wang, J. Yuan, S.M. Rocha, A.J.D. Silvestre, I.M. Marrucho, Thin porous poly(ionic liquid) coatings for enhanced headspace solid phase microextraction, Polymers (Basel). 12 (2020) 1909, https://doi.org/10.3390/polym12091909.

[13] C.L. Yiin, K.L. Yap, A.Z.E. Ku, B.L.F. Chin, S.S.M. Lock, K.W. Cheah, A.C.M. Loy, Y.H. Chan, Recent advances in green solvents for lignocellulosic biomass pretreatment: Potential of choline chloride (ChCl) based solvents, Bioresour. Technol. 333 (2021) 125195, https://doi.org/10.1016/j.biortech.2021.125195.

[14] E.S. Morais, A.M.d.C. Lopes, M.G. Freire, C.S.R. Freire, J.A.P. Coutinho, A.J.D. Silvestre, Use of ionic liquids and deep eutectic solvents in polysaccharides dissolution and extraction processes towards sustainable biomass valorization, Molecules. 25 (16) (2020) 3652, https://doi.org/10.3390/molecules25163652.

[15] A.M. Asim, M. Uroos, S. Naz, M. Sultan, G. Griffin, N. Muhammad, A.S. Khan, Acidic ionic liquids: Promising and cost-effective solvents for processing of lignocellulosic biomass, J. Mol. Liq. 287 (2019) 110943, https://doi.org/10.1016/j.molliq.2019.110943.

[16] A. Abednejad, A. Ghaee, E.S. Morais, M. Sharma, B.M. Neves, M.G. Freire, J. Nourmohammadi, A.A. Mehrizi, Polyvinylidene fluoride–Hyaluronic acid wound dressing comprised of ionic liquids for controlled drug delivery and dual therapeutic behavior, Acta Biomater. 100 (2019) 142–157, https://doi.org/10.1016/j.actbio.2019.10.007.

[17] M.K. Ali, R.M. Moshikur, R. Wakabayashi, M. Moniruzzaman, N. Kamiya, M. Goto, Biocompatible ionic liquid surfactant-based microemulsion as a potential carrier for sparingly soluble drugs, ACS Sustain. Chem. Eng. 8 (16) (2020) 6263–6272, https://doi.org/10.1021/acssuschemeng.9b0777310.1021/acssuschemeng.9b07773.s001.

[18] S. Tampucci, L. Guazzelli, S. Burgalassi, S. Carpi, P. Chetoni, A. Mezzetta, P. Nieri, B. Polini, C.S. Pomelli, E. Terreni, D. Monti, pH-responsive nanostructures based on surface active fatty acid-protic ionic liquids for imiquimod delivery in skin cancer topical therapy, Pharmaceutics. 12 (2020) 1078, https://doi.org/10.3390/pharmaceutics12111078.

[19] Alexander H. Tullo, The time is now for ionic liquids, Chem. Eng. News. 98 (2020) February 3. https://cen.acs.org/materials/ionic-liquids/time-ionic-liquids/98/i5.

[20] M. Suk, A. Haiß, J. Westphal, A. Jordan, A. Kellett, I.V. Kapitanov, Y. Karpichev, N. Gathergood, K. Kümmerer, Design rules for environmental biodegradability of phenylalanine alkyl ester linked ionic liquids, Green Chem. 22 (14) (2020) 4498–4508, https://doi.org/10.1039/D0GC00918K.

[21] D.K.A. Kusumahastuti, M. Sihtmäe, V. Aruoja, N. Gathergood, A. Kahru, Ecotoxicity profiling of a library of 24 l-phenylalanine derived surface-active ionic liquids (SAILs), Sustain. Chem. Pharm. 19 (2021) 100369, https://doi.org/10.1016/j.scp.2020.100369.

[22] W. Florio, S. Becherini, F. D'Andrea, A. Lupetti, C. Chiappe, L. Guazzelli, Comparative evaluation of antimicrobial activity of different types of ionic liquids, Mater. Sci. Eng. C. 104 (2019) 109907, https://doi.org/10.1016/j.msec.2019.109907.

[23] V.F. Scalfani, A. Al Alshaikh, J.E. Bara, Analysis of the frequency and diversity of 1,3-dialkylimidazolium ionic liquids appearing in the literature, Ind. Eng. Chem. Res. 57 (47) (2018) 15971–15981, https://doi.org/10.1021/acs.iecr.8b0257310.1021/acs.iecr.8b02573.s001.

[24] J. Hulsbosch, D.E. De Vos, K. Binnemans, R. Ameloot, Biobased ionic liquids: solvents for a green processing industry? ACS Sustain. Chem. Eng. 4 (6) (2016) 2917–2931, https://doi.org/10.1021/acssuschemeng.6b00553.

[25] S. Kirchhecker, D. Esposito, Amino acid based ionic liquids: A green and sustainable perspective, Curr. Opin. Green Sustain. Chem. 2 (2016) 28–33, https://doi.org/10.1016/j.cogsc.2016.09.001.

[26] A.M. Socha, R. Parthasarathi, J. Shi, S. Pattathil, D. Whyte, M. Bergeron, A. George, K. Tran, V. Stavila, S. Venkatachalam, M.G. Hahn, B.A. Simmons, S. Singh, Efficient biomass pretreatment using ionic liquids derived from lignin and hemicellulose, Proc. Natl. Acad. Sci. 111 (35) (2014) E3587–E3595, https://doi.org/10.1073/pnas.1405685111.

[27] B. Gaida, A. Brzęczek-Szafran, Insights into the properties and potential applications of renewable carbohydrate-based ionic liquids: a review, Molecules. 25 (2020) 3285, https://doi.org/10.3390/molecules25143285.

[28] K. Erfurt, M. Markiewicz, A. Siewniak, D. Lisicki, M. Zalewski, S. Stolte, A. Chrobok, Biodegradable surface active D-glucose based quaternary ammonium ionic liquids in the solventless synthesis of chloroprene, ACS Sustain. Chem. Eng. (2020), https://doi.org/10.1021/acssuschemeng.0c03239.

[29] V. Zullo, A. Iuliano, L. Guazzelli, Sugar-based ionic liquids: multifaceted challenges and intriguing potential, Molecules. 26 (2021) 2052, https://doi.org/10.3390/molecules26072052.

[30] D. Mondal, M. Sharma, M.V. Quental, A.P.M. Tavares, K. Prasad, M.G. Freire, Suitability of bio-based ionic liquids for the extraction and purification of IgG antibodies, Green Chem. 18 (22) (2016) 6071–6081, https://doi.org/10.1039/C6GC01482H.

[31] P. Iranpour, M. Ajamian, A. Safavi, N. Iranpoor, A. Abbaspour, S. Javanmardi, Synthesis of highly stable and biocompatible gold nanoparticles for use as a new X-ray contrast agent, J. Mater. Sci. Mater. Med. 29 (2018) 48, https://doi.org/10.1007/s10856-018-6053-5.

[32] F. Billeci, F. D'Anna, M. Feroci, P. Cancemi, S. Feo, A. Forlino, F. Tonnelli, K.R. Seddon, H.Q.N. Gunaratne, N.V. Plechkova, When functionalization becomes useful: ionic liquids with a "sweet" appended moiety demonstrate drastically reduced toxicological effects, ACS Sustain. Chem. Eng. 8 (2) (2020) 926–938, https://doi.org/10.1021/acssuschemeng.9b0550710.1021/acssuschemeng.9b05507.s001.

[33] M. Zunita, D. Wahyuningrum, Buchari, B. Bundjali, I.G. Wenten, R. Boopathy, Conversion of glucose to 5-hydroxymethylfurfural, levulinic acid, and formic acid in 1,3-dibutyl-2-(2-butoxyphenyl)-4,5-diphenylimidazolium iodide-based ionic liquid, Appl. Sci. 11 (3) (2021) 989, https://doi.org/10.3390/app11030989.

[34] D.i. Hu, M. Zhang, H. Xu, Y. Wang, K. Yan, Recent advance on the catalytic system for efficient production of biomass-derived 5-hydroxymethylfurfural, Renew. Sustain. Energy Rev. 147 (2021) 111253, https://doi.org/10.1016/j.rser.2021.111253.

[35] X. Cheng, Y. Liu, K. Wang, H. Yu, S. Yu, S. Liu, High-efficient conversion of cellulose to levulinic acid catalyzed via functional brønsted-lewis acidic ionic liquids, Catal. Lett. (2021), https://doi.org/10.1007/s10562-021-03701-w.

[36] J. Zhang, X. Zhang, M. Yang, S. Singh, G. Cheng, Transforming lignocellulosic biomass into biofuels enabled by ionic liquid pretreatment, Bioresour. Technol. 322 (2021) 124522, https://doi.org/10.1016/j.biortech.2020.124522.

[37] M.M. Seitkalieva, A.V. Vavina, A.V. Posvyatenko, K.S. Egorova, A.S. Kashin, E.G. Gordeev, E.N. Strukova, L.V. Romashov, V.P. Ananikov, Biomass-derived ionic liquids based on a 5-HMF platform chemical: synthesis, characterization, biological activity, and tunable interactions at the molecular level, ACS Sustain. Chem. Eng. 9 (9) (2021) 3552–3570, https://doi.org/10.1021/acssuschemeng.0c08790.

[38] S. Kirchhecker, S. Tröger-Müller, S. Bake, M. Antonietti, A. Taubert, D. Esposito, Renewable pyridinium ionic liquids from the continuous hydrothermal decarboxylation of furfural-amino acid derived pyridinium zwitterions, Green Chem. 17 (8) (2015) 4151–4156, https://doi.org/10.1039/C5GC00913H.

[39] S. Shahriari, L.C. Tomé, J.M.M. Araújo, L.P.N. Rebelo, J.A.P. Coutinho, I.M. Marrucho, M.G. Freire, Aqueous biphasic systems: a benign route using cholinium-based ionic liquids, RSC Adv. 3 (6) (2013) 1835–1843, https://doi.org/10.1039/C2RA22972B.

[40] A. Yokozeki, M.B. Shiflett, C.P. Junk, L.M. Grieco, T. Foo, Physical and chemical absorptions of carbon dioxide in room-temperature ionic liquids, J. Phys. Chem. B. 112 (51) (2008) 16654–16663, https://doi.org/10.1021/jp805784u.

[41] S. Stevanovic, A. Podgorsek, L. Moura, C.C. Santini, A.A.H. Padua, M.F. Costa Gomes, Absorption of carbon dioxide by ionic liquids with carboxylate anions, Int. J. Greenh. Gas Control. 17 (2013) 78–88, https://doi.org/10.1016/j.ijggc.2013.04.017.
[42] J. Avila, L.F. Lepre, C.C. Santini, M. Tiano, S. Denis-Quanquin, K. Chung Szeto, A.A.H. Padua, M. Costa Gomes, High-performance porous ionic liquids for low-pressure CO 2 capture**, Angew. Chemie Int. Ed. 60 (23) (2021) 12876–12882, https://doi.org/10.1002/anie.202100090.
[43] V. Wagner, P.S. Schulz, P. Wasserscheid, Asymmetric hydrogenation catalysis via ion-pairing in chiral ionic liquids, J. Mol. Liq. 192 (2014) 177–184, https://doi.org/10.1016/j.molliq.2013.10.025.
[44] F. Boissou, A. Mühlbauer, K. De Oliveira Vigier, L. Leclercq, W. Kunz, S. Marinkovic, B. Estrine, V. Nardello-Rataj, F. Jérôme, Transition of cellulose crystalline structure in biodegradable mixtures of renewably-sourced levulinate alkyl ammonium ionic liquids, γ-valerolactone and water, Green Chem. 16 (5) (2014) 2463–2471, https://doi.org/10.1039/C3GC42396D.
[45] S. Becherini, A. Mezzetta, C. Chiappe, L. Guazzelli, Levulinate amidinium protic ionic liquids (PILs) as suitable media for the dissolution and levulination of cellulose, New J. Chem. 43 (11) (2019) 4554–4561, https://doi.org/10.1039/C9NJ00191C.
[46] A. Mezzetta, S. Becherini, C. Pretti, G. Monni, V. Casu, C. Chiappe, L. Guazzelli, Insights into the levulinate-based ionic liquid class: synthesis, cellulose dissolution evaluation and ecotoxicity assessment, New J. Chem. 43 (33) (2019) 13010–13019, https://doi.org/10.1039/C9NJ03239H.
[47] L. Guglielmero, A. Mezzetta, L. Guazzelli, C.S. Pomelli, F. D'Andrea, C. Chiappe, Systematic synthesis and properties evaluation of dicationic ionic liquids, and a glance into a potential new field, Front. Chem. 6 (2018) 1–16, https://doi.org/10.3389/fchem.2018.00612.
[48] C. Chiappe, P. Margari, A. Mezzetta, C.S. Pomelli, S. Koutsoumpos, M. Papamichael, P. Giannios, K. Moutzouris, Temperature effects on the viscosity and the wavelength-dependent refractive index of imidazolium-based ionic liquids with a phosphorus-containing anion, Phys. Chem. Chem. Phys. 19 (12) (2017) 8201–8209, https://doi.org/10.1039/C6CP08910K.
[49] K. Moutzouris, M. Papamichael, S.C. Betsis, I. Stavrakas, G. Hloupis, D. Triantis, Refractive, dispersive and thermo-optic properties of twelve organic solvents in the visible and near-infrared, Appl. Phys. B. 116 (3) (2014) 617–622, https://doi.org/10.1007/s00340-013-5744-3.
[50] A. Mezzetta, L. Guazzelli, M. Seggiani, C.S. Pomelli, M. Puccini, C. Chiappe, A general environmentally friendly access to long chain fatty acid ionic liquids (LCFA-ILs), Green Chem. 19 (13) (2017) 3103–3111, https://doi.org/10.1039/C7GC00830A.
[51] C. Chiappe, A. Mezzetta, C.S. Pomelli, M. Puccini, M. Seggiani, Product as reaction solvent: an unconventional approach for ionic liquid synthesis, Org. Process Res. Dev. 20 (12) (2016) 2080–2084, https://doi.org/10.1021/acs.oprd.6b00302.
[52] H. Kanno, A simple derivation of the empirical rule, J. Non. Cryst. Solids. 44 (2–3) (1981) 409–413, https://doi.org/10.1016/0022-3093(81)90047-8.
[53] B. Lu, A. Xu, J. Wang, Cation does matter: how cationic structure affects the dissolution of cellulose in ionic liquids, Green Chem. 16 (3) (2014) 1326–1335, https://doi.org/10.1039/C3GC41733F.
[54] Y. Fukaya, A. Sugimoto, H. Ohno, Superior solubility of polysaccharides in low viscosity, polar, and halogen-free 1,3-dialkylimidazolium formates, Biomacromolecules. 7 (12) (2006) 3295–3297, https://doi.org/10.1021/bm060327d10.1021/bm060327d.s001.
[55] E. Gómez, N. Calvar, Á. Domínguez, E.A. Macedo, Thermal Analysis and heat capacities of 1-alkyl-3-methylimidazolium ionic liquids with NTf 2 –, TFO –, and DCA – anions, Ind. Eng. Chem. Res. 52 (5) (2013) 2103–2110, https://doi.org/10.1021/ie3012193.
[56] Y. Cao, T. Mu, Comprehensive investigation on the thermal stability of 66 ionic liquids by thermogravimetric analysis, Ind. Eng. Chem. Res. 53 (20) (2014) 8651–8664, https://doi.org/10.1021/ie5009597.
[57] M.T. Clough, K. Geyer, P.A. Hunt, J. Mertes, T. Welton, Thermal decomposition of carboxylate ionic liquids: Trends and mechanisms, Phys. Chem. Chem. Phys. 15 (2013) 20480–20495, https://doi.org/10.1039/c3cp53648c.
[58] K. Paduszyński, U. Domańska, Viscosity of ionic liquids: an extensive database and a new group contribution model based on a feed-forward artificial neural network, J. Chem. Inf. Model. 54 (5) (2014) 1311–1324, https://doi.org/10.1021/ci500206u.
[59] J.M.M. Araújo, A.B. Pereiro, F. Alves, I.M. Marrucho, L.P.N. Rebelo, Nucleic acid bases in 1-alkyl-3-methylimidazolium acetate ionic liquids: A thermophysical and ionic conductivity analysis, J. Chem. Thermodyn. 57 (2013) 1–8, https://doi.org/10.1016/j.jct.2012.07.022.
[60] S. Fendt, S. Padmanabhan, H.W. Blanch, J.M. Prausnitz, Viscosities of acetate or chloride-based ionic liquids and some of their mixtures with water or other common solvents, J. Chem. Eng. Data. 56 (1) (2011) 31–34, https://doi.org/10.1021/je1007235.
[61] C.A. Angell, Structural instability and relaxation in liquid and glassy phases near the fragile liquid limit, J. Non. Cryst. Solids. 102 (1–3) (1988) 205–221, https://doi.org/10.1016/0022-3093(88)90133-0.
[62] C.A. Angell, Formation of glasses from liquids and biopolymers, Science (80-.) 267 (5206) (1995) 1924–1935.
[63] C.A. Angell, Glass formation and glass transition in supercooled liquids, with insights from study of related phenomena in crystals, J. Non. Cryst. Solids. 354 (42–44) (2008) 4703–4712, https://doi.org/10.1016/j.jnoncrysol.2008.05.054.
[64] C.A. Angell, K.L. Ngai, G.B. McKenna, P.F. McMillan, S.W. Martin, Relaxation in glassforming liquids and amorphous solids, J. Appl. Phys. 88 (6) (2000) 3113–3157, https://doi.org/10.1063/1.1286035.
[65] D. Huang, G.B. McKenna, New insights into the fragility dilemma in liquids, J. Chem. Phys. 114 (13) (2001) 5621–5630, https://doi.org/10.1063/1.1348029.
[66] P. Sippel, P. Lunkenheimer, S. Krohns, E. Thoms, A. Loidl, Importance of liquid fragility for energy applications of ionic liquids, Sci. Rep. 5 (2015) 13922, https://doi.org/10.1038/srep13922.
[67] R. Tao, E. Gurung, M.M. Cetin, M.F. Mayer, E.L. Quitevis, S.L. Simon, Fragility of ionic liquids measured by Flash differential scanning calorimetry, Thermochim. Acta. 654 (2017) 121–129, https://doi.org/10.1016/j.tca.2017.05.008.
[68] J.J. Moura Ramos, C.A.M. Afonso, L.C. Branco, Glass transition relaxation and fragility in two room temperature ionic liquids, J. Therm. Anal. Calorim. 71 (2003) 659–666, https://doi.org/10.1023/A:1022884716750.
[69] Q. Zheng, J.C. Mauro, Viscosity of glass-forming systems, J. Am. Ceram. Soc. 100 (1) (2017) 6–25.
[70] I.M. Hodge, Strong and fragile liquids — a brief critique, J. Non. Cryst. Solids. 202 (1–2) (1996) 164–172, https://doi.org/10.1016/0022-3093(96)00151-2.
[71] M.C.C. Ribeiro, Low-frequency Raman spectra and fragility of imidazolium ionic liquids, J. Chem. Phys. 133 (2) (2010) 024503, https://doi.org/10.1063/1.3462962.
[72] G.W. Scherer, Editorial Comments on a Paper by Gordon S. Fulcher, J. Am. Ceramic Soc. 75 (5) (1992) 1060–1062.
[73] W.T. Laughlin, D.R. Uhlmann, Viscous flow in simple organic liquids, J. Phys. Chem. 76 (16) (1972) 2317–2325, https://doi.org/10.1021/j100660a023.
[74] F. Stickel, E.W. Fischer, R. Richert, Dynamics of glass-forming liquids. I. Temperature-derivative analysis of dielectric relaxation data, J. Chem. Phys. 102 (15) (1995) 6251–6257, https://doi.org/10.1063/1.469071.
[75] J.J. Moura-Ramos, N.T. Correia, The Deborah number, relaxation phenomena and thermally stimulated currents, Phys. Chem. Chem. Phys. 3 (2001) 5575–5578, https://doi.org/10.1039/b107984k.
[76] J. Jacquemin, P. Husson, A.A.H. Padua, V. Majer, Density and viscosity of several pure and water-saturated ionic liquids, Green Chem. 8 (2) (2006) 172–180, https://doi.org/10.1039/B513231B.
[77] Y. Arosa, B.S. Algnamat, C.D. Rodríguez, E.L. Lago, L.M. Varela, R. de la Fuente, Modeling the temperature-dependent material dispersion of imidazolium-based ionic liquids in the VIS-NIR, J. Phys. Chem. C. 122 (51) (2018) 29470–29478, https://doi.org/10.1021/acs.jpcc.8b0897110.1021/acs.jpcc.8b08971.s001.
[78] B.S. Algnamat, Y. Arosa, E. López Lago, R. de la Fuente, An inspection of the dispersive properties of imidazolium-based ionic liquids in the Vis-NIR, Opt. Mater. (Amst). 102 (2020) 109764, https://doi.org/10.1016/j.optmat.2020.109764.
[79] X. He, Q. Shao, W. Kong, L. Yu, X. Zhang, Y. Deng, A simple method for estimating mutual diffusion coefficients of ionic liquids-water based on an optofluidic chip, Fluid Phase Equilib. 366 (2014) 9–15, https://doi.org/10.1016/j.fluid.2014.01.003.
[80] J. Wan, Y. Zuo, Z. Wang, F. Yan, L. Ge, Z. Liang, Magnetohydrodynamic Microfluidic Drive of Ionic Liquids, J. Microelectromech. Syst. 23 (2014) 1463–1470, https://doi.org/10.1109/JMEMS.2014.2315638.
[81] X. He, Q. Shao, P. Cao, W. Kong, J. Sun, X. Zhang, Y. Deng, Electro-optical phenomena based on ionic liquids in an optofluidic waveguide, Lab Chip. 15 (5) (2015) 1311–1319, https://doi.org/10.1039/C4LC01434K.
[82] H. Zhang, C. Zhang, S. Vaziri, F. Kenarangi, Y. Sun, Microfluidic ionic liquid dye laser, IEEE Photonics J. 13 (1) (2021) 1–8, https://doi.org/10.1109/JPHOT.2020.3044861.
[83] X. Hu, S. Zhang, C. Qu, Q. Zhang, L. Lu, X. Ma, X. Zhang, Y. Deng, Ionic liquid based variable focus lenses, Soft Matter. 7 (13) (2011) 5941, https://doi.org/10.1039/c1sm05585b.
[84] J.A. Nóvoa-López, E. López Lago, M. Domínguez-Pérez, J. Troncoso, L.M. Varela, R. de la Fuente, O. Cabeza, H. Michinel, J.R. Rodríguez, Thermal refraction in ionic liquids induced by a train of femtosecond laser pulses, Opt. Laser Technol. 61 (2014) 1–7, https://doi.org/10.1016/j.optlastec.2014.01.017.
[85] V.C. Ferreira, G. Marin, J. Dupont, R.R.B. Correia, Nonlinear and thermo-optical characterisation of bare imidazolium ionic liquids, J. Phys. Condens. Matter. 33 (9) (2020) 095101, https://doi.org/10.1088/1361-648X/abcdaf.
[86] B.-R. Hyun, S.V. Dzyuba, R.A. Bartsch, E.L. Quitevis, Intermolecular dynamics of room-temperature ionic liquids: femtosecond optical Kerr effect measurements on 1-alkyl-3-methylimidazolium bis((trifluoromethyl)sulfonyl)imides, J. Phys. Chem. A. 106 (2002) 7579–7585, https://doi.org/10.1021/jp0141575.
[87] N. Chandrasekhar, O. Schalk, A.-N. Unterreiner, Femtosecond UV excitation in imidazolium-based ionic liquids, J. Phys. Chem. B. 112 (49) (2008) 15718–15724, https://doi.org/10.1021/jp804861z.
[88] V.V. Chaban, O.V. Prezhdo, Polarization versus temperature in pyridinium ionic liquids, J. Phys. Chem. B. 118 (48) (2014) 13940–13945, https://doi.org/10.1021/jp5089788.